UDC 551.510.53.534:551.513:551.509.313

Numerical Experiments on the Steady-State Meridional Structure and Ozone Distribution in the Stratosphere

V. R. KRISHNA RAO—*Atmospheric Environment Service of Canada, Toronto, Ontario*

ABSTRACT—A two-dimensional circulation model of the stratosphere, incorporating the mutual interrelationships between radiation, photochemistry, and seasonal transport processes, was run under steady-state assumptions to study seasonal variations. The large-scale, quasi-horizontal eddy processes were parameterized in terms of time-zonal mean temperature and ozone mixing ratio using the generalized diffusion formulation on a sloping surface.

The computed distributions of temperature and ozone mixing ratio in the meridional plane show satisfactory agreement with the observations in different seasons, thus accounting for the considerable discrepancies between the radiative-photochemical equilibrium state and observations. The significant jetlike features such as westerlies in winter and tropical easterlies in summer are well-reproduced in the upper stratosphere.

As a consequence of the generalized diffusion, the mean meridional motions developed the two-cell structure typical of that found in recent observational studies of the winter lower stratosphere.

Quasi-horizontal eddies and mean meridional motions contributed significantly to heat and ozone budgets, whereas the vertical eddies had little effect except to transport ozone downward in the winter lower stratosphere.

1. INTRODUCTION

Since the publication of Chapman's (1930) paper on the photochemical formation of ozone, there have been numerous attempts (Wulf and Deming 1936, Craig 1950, Dütsch 1946, and others) to explain the discrepancies between photochemical theory and the observations as revealed by the classical ozone measurements by Dobson et al. (1927). It is now generally accepted that much of the discrepancy is due to atmospheric transport processes.

One of the first attempts to combine the nonphotochemical processes with the photochemistry of ozone in a numerical model was that of Prabhakara (1963). He obtained the steady-state solution for the ozone equation in the meridional plane by balancing the photochemical effects with the ozone transports by the motion terms. The specified mean meridional motions were based on calculations by Murgatroyd and Singleton (1961), and the large-scale eddy effects were parameterized using the Fickian-type diffusion formulation. Although moderate success was achieved in simulating the gross features of the observed ozone distribution, little insight was obtained on the operation of the transport and physical processes because of over-simplification of the complex interactions among ozone, temperature, and circulation.

Recently, there have been attempts to model the winter stratosphere with a more realistic approach. Joint radiative, photochemical, and dynamical time-integration studies of the winter stratosphere by Byron-Scott (1967) and Clark (1970) reveal the importance of the large-scale wave disturbances for the poleward transport of heat and ozone. The primary purpose of these studies, however, was to simulate the stratospheric winter warming phenomenon.

The most detailed investigations of the diffusion of tracer material in the winter stratosphere were those of Hunt and Manabe (1968) and Hunt (1969). The model used for those investigations was an 18-level verison of the general circulation model of Smagorinsky et al. (1965). Despite the omission of the thermal coupling between the radiative and photochemical sources and sinks, they found that both large-scale eddies and mean meridional motions were important to the poleward transports of the trace substances such as ozone. However, these authors themselves agree that their studies provide no information on the seasonal variations of ozone and other such properties in the stratosphere.

In this study, the major interactions between radiative, photochemical, and transport processes are retained in the meridional plane, and the necessary modeling simplification is achieved by parameterizing the eddy circulation in terms of generalized diffusion related to time-zonal mean properties (Reed and German 1965). The relative roles of the mean meridional motions and the parameterized eddies in maintaining the seasonal distributions of temperature, winds, and ozone in the presence of radiative and photochemical sources and sinks are the major focus of this paper.

2. THE MODEL

Vertical Coordinate

To retain the advantage of pressure as a vertical coordinate and to achieve adequate vertical resolution in the stratosphere, we defined the coordinate for this experiment, by the parameter Z [following Eliassen (1949)], where

$$Z=-\ln\frac{p}{p_s}. \tag{1}$$

In eq (1), p is the pressure, and p_s is the reference pressure taken arbitrarily at 70 mb.

Averaged Equations

The atmospheric evolutions in this experiment are represented by the two horizontal equations of motion, and the hydrostatic, continuity, thermodynamic and ozone equations. Following the method of Reynolds (1894), these are averaged with respect to time, t, and longitude, λ, using the definitions

$$(\overline{\ })=\frac{1}{2\pi\tau}\int^{\tau}\int^{2\pi}(\ )\,d\lambda dt$$

and

$$(\ )=(\overline{\ })+(\ )'$$

where $(\overline{\ })$ denotes the time-zonal average of any quantity $(\ )$ over a period τ and $(\ )'$ represents the departure from the time-zonal average. The averaging period chosen here is comparable to the duration of a season, and this removes tidal and short-period fluctuations.

In the second equation of motion, the advection and local acceleration terms are assumed to be small compared to the Coriolis and pressure gradient forces; thus the flow remains approximately in geostrophic balance except near the Equator. Using these approximations and neglecting viscous effects, we can write the final averaged equations of zonal momentum, continuity, thermodynamics, thermal wind, and ozone under steady-state conditions as

$$\frac{\bar{v}}{a\cos\phi}\frac{\partial}{\partial\phi}(\bar{u}\cos\phi)+\bar{\dot{Z}}\frac{\partial\bar{u}}{\partial Z}-f\bar{v}+\frac{1}{a\cos^2\phi}\frac{\partial}{\partial\phi}(\overline{v'u'}\cos^2\phi)+\frac{\partial}{\partial Z}(\overline{\dot{Z}'u'})-\overline{\dot{Z}'u'}=0, \tag{2}$$

$$\frac{1}{a}\frac{\partial\bar{v}}{\partial\phi}+\frac{\partial\bar{\dot{Z}}}{\partial Z}-\bar{\dot{Z}}-\bar{v}\frac{\tan\phi}{a}=0, \tag{3}$$

$$\frac{\bar{v}}{a}\frac{\partial\bar{\theta}}{\partial\phi}+\bar{\dot{Z}}\frac{\partial\bar{\theta}}{\partial Z}+\frac{1}{a\cos\phi}\frac{\partial}{\partial\phi}(\overline{v'\theta'}\cos\phi)+\frac{\partial}{\partial Z}(\overline{\dot{Z}'\theta'})-\overline{\dot{Z}'\theta'}-\left(\frac{p_0}{p}\right)^{\kappa}\frac{\bar{\dot{Q}}}{c_p}=0, \tag{4}$$

$$f\frac{\partial\bar{u}}{\partial Z}+\frac{R}{a}\frac{\partial\bar{T}}{\partial\phi}=0, \tag{5}$$

and

$$\frac{\bar{v}}{a}\frac{\partial\bar{\chi}}{\partial\phi}+\bar{\dot{Z}}\frac{\partial\chi}{\partial Z}+\frac{1}{a\cos\phi}\frac{\partial}{\partial\phi}(\overline{v'\chi'}\cos\phi)+\frac{\partial}{\partial Z}(\overline{\dot{Z}'\chi'})-\overline{\dot{Z}'\chi'}-\bar{\dot{P}}=0, \tag{6}$$

where,

a = radius of the earth,
c_p = specific heat at constant pressure,
f = Coriolis parameter,
p_o = pressure at 1000 mb,
$\dot{P}$ = rate at which ozone is produced from photochemical processes,
$\dot{Q}$ = rate of heat addition per unit mass due to radiation,
R = gas constant for dry air,
T = temperature,
u = eastward wind component,
v = northward wind component,
$\dot{Z}$ = upward wind component
θ = potential temperature,
$\kappa = R/c_p$,
ϕ = latitude, and
χ = ozone mixing ratio.

Equations (2)–(6) constitute a system of five equations in five dependent variables; namely $\bar{u}$, $\bar{v}$, $\bar{\dot{Z}}$, $\bar{\theta}$, and $\bar{\chi}$, and are sufficient to close the system mathematically with proper boundary conditions, provided $\bar{\dot{Q}}$, $\bar{\dot{P}}$, and the eddy fluxes of heat, momentum, and ozone can be expressed as functions of the dependent variables.

A parameterization suitable for heat and ozone transports occurring on a meridionally sloping surface (Reed and German 1965) was used to express the fluxes in terms of the averaged dependent variables. This representation is capable of producing meridional counter-gradient heat fluxes in the lower stratosphere. As an example, the expression given by Reed and German for the eddy flux of heat in the meridional direction can be written as

$$\overline{v'\theta'}=-K_{yy}\left(1-\frac{\bar{\alpha}}{\bar{\beta}}\right)\frac{\partial\bar{\theta}}{\partial y} \tag{7}$$

where $\bar{\alpha}$ represents the slope of the mixing path, $\bar{\beta}$ represents the slope of the $\bar{\theta}$ surface, and K_{yy} is the coefficient of eddy diffusion in the y direction.

One can see from eq (7) that the flux is countergradient if $\bar{\alpha} > \bar{\beta}$. If on the other hand, $\bar{\alpha} < \bar{\beta}$, the heat flow is down the gradient. Finally, when $\bar{\alpha} = 0$, eq (7) reduces to a familiar expression for Fickian diffusion.

Using the definition for β,

$$\bar{\beta}\simeq\tan\bar{\beta}=-\frac{\dfrac{\partial\bar{\theta}}{\partial y}}{\dfrac{\partial\bar{\theta}}{\partial z}},$$

we can write the horizontal and vertical heat fluxes as

$$\overline{v'\theta'}=-\left(K_{yy}\frac{\partial\bar{\theta}}{\partial y}+K_{yz}\frac{\partial\bar{\theta}}{\partial z}\right)$$

and (8)

$$\overline{H\dot{Z}'\theta'}=-\left(K_{zz}\frac{\partial\bar{\theta}}{\partial z}+K_{yz}\frac{\partial\bar{\theta}}{\partial y}\right)$$

where $K_{yz}=\bar{\alpha}\,K_{yy}$, the cross-component eddy diffusion coefficient, H is the scale height, z is the geometric height, and $K_{zz}=(\bar{\alpha}^2+\overline{\alpha'^2})K_{yy}$, the vertical eddy diffusion coefficient. Assuming the large-scale eddy mixing of ozone takes place in the same manner as heat, we have

$$\overline{v'\chi'}=-\left(K_{yy}\frac{\partial\bar{\chi}}{\partial y}+K_{yz}\frac{\partial\bar{\chi}}{\partial z}\right)$$

and (9)

$$\overline{H\dot{Z}'\chi'}=-\left(K_{zz}\frac{\partial\bar{\chi}}{\partial z}+K_{yz}\frac{\partial\bar{\chi}}{\partial y}\right).$$

The seasonal and latitudinal distributions of K_{yy}, K_{yz}, and K_{zz} are taken from Reed and German (1965) for the lower stratosphere. Lacking such information at higher levels in the stratosphere, we used these values as the basis for the flux calculation in the model. However, an attempt has been made to derive K_{yy} at higher levels using the wind statistics information given by Newell (1963) with the assumption that K_{yy} is proportional to the variance of the meridional wind component.

Reed and German's choice of the diffusion coefficients to calculate the heat transports in the model is justified by the fact that the coefficients have been derived based on heat flux and temperature data. There appears to be some question, however, whether one could use the same form of diffusion and the coefficients to describe the ozone transports in the model. Preliminary calculations show that the assumption on the form of diffusion of ozone is satisfactory, although the coefficients based on heat flux data may have the effect of slightly overestimating the ozone transports in the meridional direction.

Momentum fluxes are parameterized as related to the meridional thermal gradients (Williams and Davies 1965) consistent with the thesis that the meridional momentum flux is mainly controlled by the baroclinic processes. Thus, following Williams and Davies we have

$$\overline{v'u'}=-K_{ym}\frac{\partial\bar{T}}{\partial y}$$

and (10)

$$\overline{H\dot{Z}'u'}=-K_{zm}\frac{\partial\bar{u}}{\partial z}$$

where

$$K_{ym}(\mathrm{cm^3\cdot deg^{-1}\cdot s^{-2}})=0.65\times10^7\Omega K_{yy}$$

and

$$K_{zm}(\mathrm{cm^2\cdot s^{-1}})=K_{zz}.$$

The symbol Ω represents the angular velocity of the earth.

Although the Williams and Davies choice is more appropriate for a baroclinically active layer ($\alpha/\beta<1$), one can extend it to a passive system ($\alpha/\beta>1$) by introducing the concept of negative eddy viscosity ($-K_{ym}$) and see whether the comparison of the model results with the observations may shed some light on the physical justification of the original assumption.

Substituting eq (8), (9), and (10) for eddy fluxes in eq (4), (6), and (2), respectively, we obtain

$$\left(\frac{\partial\bar{u}}{\partial y}-\bar{u}\frac{\tan\phi}{a}-f\right)\bar{v}+\bar{\dot{Z}}\frac{\partial\bar{u}}{\partial\bar{Z}}-\frac{\partial}{\partial y}\left(K_{ym}\frac{\partial\bar{T}}{\partial y}\right)$$
$$-\frac{1}{H}\frac{\partial}{\partial\bar{Z}}\left(\frac{K_{zm}}{H}\frac{\partial\bar{u}}{\partial\bar{Z}}\right)+\frac{K_{zm}}{H^2}\frac{\partial\bar{u}}{\partial\bar{Z}}+2\frac{\tan\phi}{a}K_{ym}\frac{\partial\bar{T}}{\partial y}=0, \quad (11)$$

$$\bar{v}\frac{\partial\bar{\theta}}{\partial y}+\bar{\dot{Z}}\frac{\partial\bar{\theta}}{\partial\bar{Z}}-\frac{\partial}{\partial y}\left(K_{yy}\frac{\partial\bar{\theta}}{\partial y}+\frac{K_{yz}}{H}\frac{\partial\bar{\theta}}{\partial\bar{Z}}\right)$$
$$-\frac{1}{H}\frac{\partial}{\partial\bar{Z}}\left(\frac{K_{zz}}{H}\frac{\partial\bar{\theta}}{\partial\bar{Z}}+K_{yz}\frac{\partial\bar{\theta}}{\partial y}\right)+\frac{1}{H}\left(\frac{K_{zz}}{H}\frac{\partial\bar{\theta}}{\partial\bar{Z}}+K_{yz}\frac{\partial\bar{\theta}}{\partial y}\right)$$
$$+\frac{\tan\phi}{a}\left(K_{yy}\frac{\partial\bar{\theta}}{\partial y}+\frac{K_{yz}}{H}\frac{\partial\bar{\theta}}{\partial\bar{Z}}\right)-\left(\frac{p_0}{p}\right)^{\kappa}\frac{\bar{\dot{Q}}}{c_p}=0, \quad (12)$$

and

$$\bar{v}\frac{\partial\bar{\chi}}{\partial y}+\bar{\dot{Z}}\frac{\partial\bar{\chi}}{\partial\bar{Z}}-\frac{\partial}{\partial y}\left(K_{yy}\frac{\partial\bar{\chi}}{\partial y}+\frac{K_{yz}}{H}\frac{\partial\bar{\chi}}{\partial\bar{Z}}\right)$$
$$-\frac{1}{H}\frac{\partial}{\partial\bar{Z}}\left(\frac{K_{zz}}{H}\frac{\partial\bar{\chi}}{\partial\bar{Z}}+K_{yz}\frac{\partial\bar{\chi}}{\partial y}\right)+\frac{1}{H}\left(\frac{K_{zz}}{H}\frac{\partial\bar{\chi}}{\partial\bar{Z}}+K_{yz}\frac{\partial\bar{\chi}}{\partial y}\right)$$
$$+\frac{\tan\phi}{a}\left(K_{yy}\frac{\partial\bar{\chi}}{\partial y}+\frac{K_{yz}}{H}\frac{\partial\bar{\chi}}{\partial\bar{Z}}\right)-\bar{\dot{P}}=0. \quad (13)$$

Since the calculations of $\bar{\dot{Q}}$ and $\bar{\dot{P}}$ will be made using the actual temperature, it is more convenient to transform eq (12) in terms of the actual temperature using the following relationships between θ and T:

$$\bar{\theta}=\bar{T}\left(\frac{p_0}{p}\right)^{\kappa} \quad (14)$$

and

$$\frac{\partial\bar{\theta}}{\partial\bar{Z}}=\left(\frac{p_0}{p}\right)^{\kappa}\left(\frac{\partial\bar{T}}{\partial\bar{Z}}+\kappa\bar{T}\right). \quad (15)$$

When eq (14) and (15) are substituted in eq (12), the thermodynamic energy equation becomes

$$\bar{v}\frac{\partial\bar{T}}{\partial y}+\bar{\dot{Z}}\left(\frac{\partial\bar{T}}{\partial\bar{Z}}+\kappa\bar{T}\right)-\frac{\partial}{\partial y}\left(K_{yy}\frac{\partial\bar{T}}{\partial y}+\frac{K_{yz}}{H}\frac{\partial\bar{T}}{\partial\bar{Z}}+\frac{K_{yz}}{H}\kappa\bar{T}\right)$$
$$-\frac{1}{H}\frac{\partial}{\partial\bar{Z}}\left(\frac{K_{zz}}{H}\frac{\partial\bar{T}}{\partial\bar{Z}}+\frac{K_{zz}}{H}\kappa\bar{T}+K_{yz}\frac{\partial\bar{T}}{\partial y}\right)$$
$$+\frac{1}{H}\left(\frac{K_{zz}}{H}\frac{\partial\bar{T}}{\partial\bar{Z}}+\frac{K_{zz}}{H}\kappa\bar{T}+K_{yz}\frac{\partial\bar{T}}{\partial y}\right)$$
$$+\frac{\tan\phi}{a}\left(K_{yy}\frac{\partial\bar{T}}{\partial y}+\frac{K_{yz}}{H}\frac{\partial\bar{T}}{\partial\bar{Z}}+\frac{K_{yz}}{H}\kappa\bar{T}\right)-\frac{\bar{\dot{Q}}}{c_p}=0. \quad (16)$$

Discrete Vertical and Horizontal Structure of the Model

The two-dimensional grid used for the numerical computations is shown in figure 1. It runs from 10 km to 55 km in the vertical and from 85°S (negative) to 85°N (positive) in the horizontal, and the poles represent the lateral boundaries. In the vertical, the finite-difference net consists of 16 discrete levels separated by a constant $\Delta Z=0.4236$. This corresponds to a height increment of

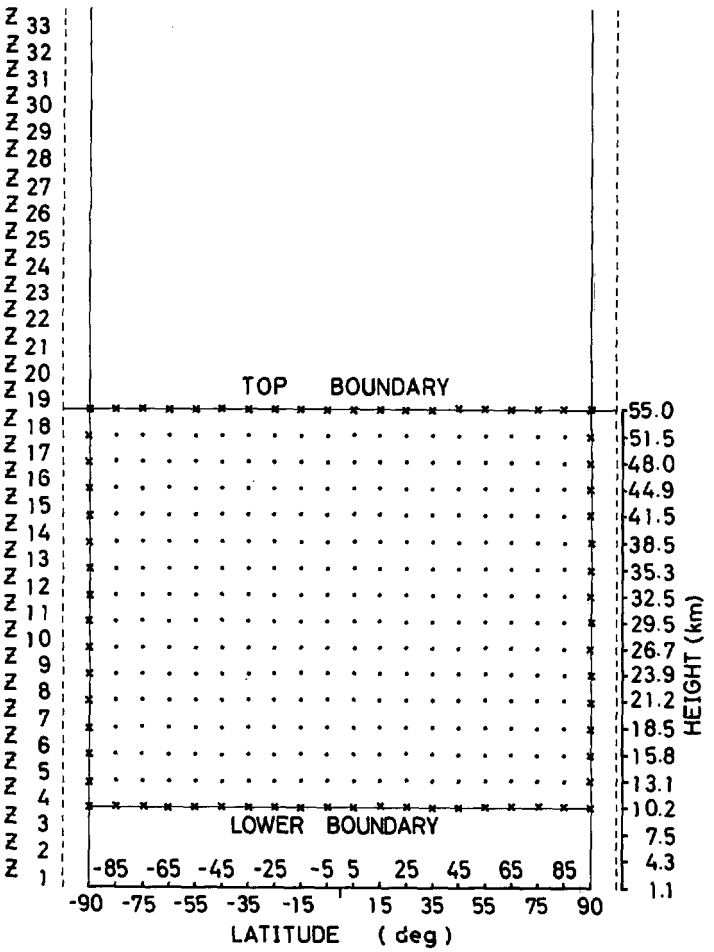

FIGURE 1.—Two dimensional grid used for numerical calculations in the model. The boundaries of the model region are marked by xs. The vertical dashed lines are the imaginary arrays outside the poles.

about 3 km in the U.S. Standard Atmosphere. In the meridional direction, the grid spacing is 10° of latitude.

Boundary Conditions

The boundary conditions applied to the equations are that both temperatures and ozone mixing ratios are specified at the lower and upper boundaries and the conditions of zero horizontal flux are assumed at both poles and at all levels. The seasonal values of $\bar{u}$ are specified at 10 km and the $\bar{\dot{Z}}$ values based on the thermal equilibrium (Murgatroyd and Singleton 1961) are used at the top boundary.

For the purpose of solving the zonal momentum equation in conjunction with the equation of continuity, we assume that both $\bar{u}$ and $\bar{v}$ are antisymmetric with respect to the poles. Unless this condition is maintained, there would be infinite divergence and vorticity at the poles due to the spherical geometry of the earth. The specification based on seasonal climatological values lacks the rigor of physical argument. However, the sensitivity of the solution in the interior of each of these boundary conditions has been tested by varying the values at the boundary.

3. PHOTOCHEMICAL AND RADIATIVE CONSIDERATIONS

The photochemical source term, $\dot{P}$, in the ozone equation and the radiative heating term, $\dot{Q}/c_p$, in the thermodynamic energy equation are computed by methods similar to those of Leovy (1964) and Byron-Scott (1967). The methods are reviewed briefly in the context of the present experiment.

The Ozone Photochemical Source Term, $\dot{P}$

Assuming that only reactions involving oxygen allotropes and a chemically inert background gas are significant in the atmospheric ozone balance, one can show (Lindzen and Goody 1965, Brewer 1966) that the ozone source term can be written in the form

$$\dot{P}=aq_2-b(p)\left(\frac{K_{13}}{K_{12}}\right)q_3T\chi^2 \tag{17}$$

where

$$a=2\left(\frac{\rho_2}{\rho_{air}}\right)\frac{M_3}{M_2}$$

and

$$b(p)=2\frac{MM_2R}{\left(\frac{\rho_2}{\rho_{air}}\right)M_3p}.$$

In the above expressions, M, M_2, and M_3 denote the molecular masses of air, oxygen, and ozone, respectively, and ρ_2 is the density of oxygen. Although the Chapman theory can be questioned on a number of points based on recent developments in ozone photochemistry (Hunt 1966, Johnston 1971), it is still the dominant photochemical mechanism in the stratosphere and is compatible with the nature of the experiment in this study.

The ratio of the reaction rate coefficients (K_{13}/K_{12}) is strongly temperature dependent and is generally expressed as

$$\frac{K_{13}}{K_{12}}=S_1\exp\left(-\frac{S_2}{T}\right) \tag{18}$$

where S_1 and S_2 are constants normally determined from chemical laboratory experiments. The values $S_1=0.255\times10^{25}$ and $S_2=3000$, adopted in the present photochemical calculations, are taken from London (1967).

Incorporating eq (18) into (17), we can write the ozone source term as

$$\dot{P}=aq_2-S_1b(p)q_3T\exp\left(-\frac{S_2}{T}\right)\chi^2. \tag{19}$$

If $I_{o\nu}$ is the intensity of the direct solar beam at the outer limit of the atmosphere [given in photons· $cm^{-2}\cdot s^{-1}\cdot$(wave no.)$^{-1}$], $\alpha_2(\nu)+p\alpha_4(\nu)$, $\alpha_3(\nu)$, and β_m are the pressure-dependent absorption cross section of molecular oxygen, the absorption cross section for ozone, and the scattering cross section for air, respectively; x_2, x_3, and x_m are the total numbers of oxygen, ozone, and air molecules above a horizontal square centimeter situated at level Z. Finally, if e_2 (ν) and e_3 (ν) are the quantum yields or efficiencies for oxygen and ozone dissociation, then the dissociation

rates q_2 and q_3 (Byron-Scott 1967) are given by

$$q_2(Z)=d\int_{\nu>41{,}300\ \mathrm{cm}^{-1}} e_2(\nu)[\alpha_2(\nu)+\tilde{p}(Z,\infty)\alpha_4(\nu)]I_{o\nu} \times\exp\{-[\alpha_2(\nu)x_2(Z)+\tilde{p}(Z,\infty)\alpha_4(\nu)x_2(Z)+\alpha_3(\nu)x_3(Z)+\beta_m(\nu)x_m(Z)]\sec\bar{\zeta}\}d\nu \quad (20)$$

and

$$q_3(Z)=d\int_{\nu>8{,}620\ \mathrm{cm}^{-1}} e_3(\nu)\alpha_3(\nu)I_{o\nu}\exp\{-[\alpha_2(\nu)x_2(Z)+\tilde{p}(Z,\infty)\alpha_4(\nu)x_2(Z)+\alpha_3(\nu)x_3(Z)+\beta_m(\nu)x_m(Z)]\sec\bar{\zeta}\}d\nu \quad (21)$$

where $\sec\bar{\zeta}$ is the mean zenith angle between sunrise and sunset at a given latitude and season, d is the fraction of the day that the sun spends above the astronomical horizon, and $\tilde{p}\ (Z,\ \infty)$ represents the oxygen-weighted mean pressure for the layer between level Z and ∞. For the details on calculating $\sec\bar{\zeta}$, d, $\tilde{p}(Z,\infty)$, x_2, x_3, and x_m, the reader is referred to Rao (1970).

The spectral data on $I_{o\nu}$, $\alpha_2(\nu)$, $\alpha_3(\nu)$, $\beta_m(\nu)$, and $e_2(\nu)$ required to evaluate q_2 and q_3 in the above equations were taken from Byron-Scott (1967). The spectral domain considered covers the wave number range from 13,500 cm^{-1} to 59,375 cm^{-1}. Contained in the range are the Hartley (2000–3000 Å), Huggins (3100–3400 Å), and Chappius (4500–7500 Å) bands of ozone and Herzberg continuum and Shumann-Runge of molecular oxygen.

The Radiative Heating Term, $\dot{Q}/c_p$

The main components of heating contributing to the sources and sinks in the thermodynamic energy equation in the stratosphere are the heating due to absorption of short-wave radiation by ozone and heating or cooling due to exchange of long-wave terrestrial radiation in the 9.6-μm band of ozone and by the 15-μm band of CO_2. Thus,

$$\frac{\dot{Q}}{c_p}=\frac{\dot{Q}_{\mathrm{SW}}}{c_p}+\frac{\dot{Q}_{\mathrm{O_3}}}{c_p}+\frac{\dot{Q}_{\mathrm{CO_2}}}{c_p}. \quad (22)$$

If $\chi(Z)$ is the mixing ratio of ozone at a level Z and $h\nu$ is the average energy of a photon, then, assuming that the quantum efficiency for ozone is unity, the heating rate due to absorption of short-wave radiation by ozone in °K/s at any specific level is given by

$$\frac{\dot{Q}_{\mathrm{SW}}(Z)}{c_p}=\frac{h\chi(Z)[q_3(Z)\nu]}{c_p M_3}$$

where h is Plank's constant.[1]

The method employed in the present calculations to obtain $\dot{Q}_{\mathrm{O_3}}/c_p$ was developed by Clark (1963); it is based on the laboratory measurements of mean absorptivities for the 9.6-μm band of ozone by Walshaw (1957). The details of the method are given by Rao (1970.)

Taking into account the fixed distribution of the absorber, we used the same procedure to compute CO_2 cooling rates (i.e., $\dot{Q}_{\mathrm{CO_2}}/c_p$) for various levels in the model as we used in the case of the 9.6-μm ozone band, except that the absorptivity matrix is computed using the empirical formulas given by Howard et al. (1955) for the integrated absorption of the 15-μm CO_2 band (Rao 1970).

[1] The multiplication of $q_3(Z)$ by ν should be achieved within the integral of eq (21).

4. METHOD OF NUMERICAL SOLUTION

To describe the numerical procedure using the method of successive approximations, we let $v^n_{i,j}$, $Z^n_{i,j}$, $T^n_{i,j}$, $u^n_{i,j}$, and $\chi^n_{i,j}$ represent the nth-order approximation. Substituting $u^n_{i,j}$ and $T^n_{i,j}$ in the spatial finite-difference analog of the zonal momentum equation [eq (11)], one can obtain $v^{n+1}_{i,j}$. Using the corrected values of $v^{n+1}_{i,j}$ in the equation of continuity, we can write the $(n+1)$th approximation for $\dot{Z}$ as

$$\dot{Z}^{n+1}_{i,j}=(\dot{Z}_T)_i e^{z_j-z_T}+e^{z_j}\sum_{k=j}^{k=19} w_k e^{-z_k}\left(\frac{v^{n+1}_{i+1,k}-v^{n+1}_{i-1,k}}{2\Delta y}-\frac{v^{n+1}_{i,k}\tan\phi_i}{a}\right)\Delta Z \quad (23)$$

where $(\dot{Z}_T)$ are the nondimensional vertical motions specified at the upper boundary, $w_k=1$ if $k\neq j$ or 19, and $w_k=1/2$ if $k=j$ or 19.

The corrected fields, $v^{n+1}_{i,j}$ and $\dot{Z}^{n+1}_{i,j}$, are now used to solve the heat equation [eq (16)] for the $(n+1)$th approximation of temperature. The well-known Liebmann relaxation technique is employed, and the computational procedure is basically similar to that described in Thompson (1961), though not in all details. From the sequential method of relaxation, the new approximation for the temperature field is given by

$$T^{n+1}_{i,j}=T^n_{i,j}+\frac{\alpha_r}{\Sigma(W_T)_{i,j}}R^{n,n+1}_{i,j} \quad (24)$$

where α_r is the relaxation coefficient. With respect to the eq (16), $R^{n,n+1}_{i,j}$ represents residues at each gridpoint, and $\Sigma(W_T)_{i,j}$ denotes the sum total of the weights given to the central point (i, j) in various terms of the equation.

The finite-difference scheme adopted here to obtain the residues from eq (16) involves central differencing for both second- and first-order derivatives of diffusion terms and the Lelivier (Richtmyer 1957) method of windward-side difference approximation for the advection terms using noncentered differences. The upstream differencing introduces additional diffusion into the system, which lacks physical argument. However, the scheme was found essential to control the numerical calculations in the model. After applying a similar procedure to the ozone equation [eq (13)], we can write the $(n+1)$th approximation for the ozone mixing ratio as

$$\chi^{n+1}_{i,j}=\chi^n_{i,j}+\frac{\alpha_r}{\Sigma(W_\chi)_{i,j}}(R_\chi)^{n,n+1}_{i,j}. \quad (25)$$

Finally, from the thermal wind equation [eq (5)] we have

$$u^{n+1}_{i,j}=(u_{\mathrm{LB}})_i+\frac{R}{f_i}\sum_{k=j}^{k=4} w_k\frac{(T^{n+1}_{i+1,k}-T^{n+1}_{i-1,k})\Delta Z}{2\Delta y} \quad (26)$$

where, $(u_{LB})_i$ are the specified values of the zonal wind at the lower boundary, $w_k=1$ if $k\neq j$ or 4, and $w_k=1/2$ if $k=j$ or 4.

Until now, we have described the procedure to compute the new approximations for all the variables once for the entire grid. After computing the new radiative and photochemical source terms from $T_{i,j}^{n+1}$ and $\chi_{i,j}^{n+1}$ at the beginning of each iteration, the entire grid is scanned repeatedly on all the variables and the successive approximations are computed until the following convergence criteria are satisfied:

$$\left|\frac{v_{i,j}^{n+1}-v_{i,j}^{n}}{v_{i,j}^{n+1}}\right| \leq 0.005,$$

$$\left|\frac{\dot{Z}_{i,j}^{n+1}-\dot{Z}_{i,j}^{n}}{\dot{Z}_{i,j}^{n+1}}\right| \leq 0.005,$$

$$\left|\frac{T_{i,j}^{n+1}-T_{i,j}^{n}}{T_{i,j}^{n+1}}\right| \leq 0.00001,$$

$$\left|\frac{u_{i,j}^{n+1}-u_{i,j}^{n}}{u_{i,j}^{n+1}}\right| \leq 0.0001,$$

and

$$\left|\frac{\chi_{i,j}^{n+1}-\chi_{i,j}^{n}}{\chi_{i,j}^{n+1}}\right| \leq 0.0001.$$

To obtain a convergent solution, one must satisfy the ellipticity criterion for the system of equations. This problem has been overcome by ellipticizing the system. By combining the zonal momentum, thermodynamic, thermal wind, and continuity equations, we derived the necessary (not sufficient) condition for the system to be elliptic. This can be written in the following form:

$$\frac{R\left(\frac{\partial\bar{T}}{\partial Z}+\kappa\bar{T}\right)\left(1-\frac{1}{f}\frac{\partial\bar{u}}{\partial y}\right)}{\left(\frac{\partial\bar{u}}{\partial Z}\right)^2}>1.$$

5. FINAL DESIGN OF THE NUMERICAL EXPERIMENT

Four experiments were performed for the summer and winter seasons. In the first experiment (case 1), the transport processes were completely suppressed and a simple radiative-photo chemical equilibrium solution for temperature and ozone mixing ratio was obtained. In case 2, both large-scale eddy effects and mean meridional motions were incorporated, but the linear temperature approximation was used to compute long-wave heating components in the heat equation (Leovy 1964, Lindzen and Goody 1965). With this approximation we can write

$$\frac{Q_{O_3}}{c_p}+\frac{Q_{CO_2}}{c_p}=T_s-cT \qquad (27)$$

where T_s and c denote the standard temperature and the relaxation time for infrared cooling, respectively. The values of T_s and c were taken from Hering et al. (1967).

Case 3 was the same as case 2 except that the long-wave heating components were computed in a detailed manner from the physical considerations. In cases 2 and 3, the eddy transfer coefficients, K_{yy}, K_{yz}, and K_{zz}, were varied only with latitude and season as shown in table 1. Case 4 is the same as case 2 except that K_{yy} and K_{yz} were varied (Rao 1970) with respect to height as well as latitude and season.

Case 2- and 3-type experiments were also extended to the spring and fall seasons in a straightforward manner, by changing the declination of the sun and by choosing diffusion coefficients and boundary fields for these seasons. The diffusion coefficients were again taken from Reed and German (table 1); as mentioned earlier, they were derived based on heat flux and temperature data in the stratosphere.

6. DISCUSSION OF THE NUMERICAL RESULTS

Radiative-Photochemical Equilibrium

The meridional cross sections of the radiative-photochemical equilibrium temperature and ozone mixing ratio appear in figures 2 and 3 for the summer and winter seasons. Since the solar radiation does not enter into the short-wave heating or the photochemical calculations beyond 65°N in the winter hemisphere, it was not possible to compute the equilibrium distribution of ozone north of 65°N. The solar radiation has, of course, played an important role in determining the temperature increase with height and in the stratopause formation in the summer hemisphere.

Comparison of figure 2 with observations by Murgatroyd (1957) shows that there are significant differences between the equilibrium and the observed distribution of temperature in the meridional plane, particularly in the winter season and also in the lower stratosphere during the summer. For example, the computed equilibrium distribution does not indicate a temperature increase from the Tropics to higher latitudes in the lower stratosphere as shown by the observations in both hemispheres (Murgatroyd 1957). In fact, the computed variation in the lower stratosphere is in the opposite direction. Furthermore, the equilibrium temperatures in the winter stratosphere are unrealistic when compared with the observations.

Figure 4 represents a meridional cross section of ozone mixing ratio for the summer and winter seasons as determined from observations obtained by the North American ozonesonde network (Hering and Borden 1964). Comparison of the equilibrium distribution of ozone mixing ratio (fig. 3) with the observations reveals that the observed distribution cannot be explained by radiative-photochemical calculations alone. Note, for example, that the computed values of ozone mixing ratio in the lower stratosphere are substantially lower than those observed, particularly in the high latitudes in both hemispheres, resulting in the opposite latitudinal variation of ozone. This strongly suggests the importance of meteorological transports in determining the ozone distribution in the lower stratosphere.

In the upper stratosphere, the ozone measurements are less reliable; however, the computed values in summer seem to agree with the observations, suggesting that the

TABLE 1.—*Latitudinal distribution of eddy diffusion coefficients K_{yy}, K_{yz}, and K_{zz} for different seasons*

	Latitude (degree)								
	5	15	25	35	45	55	65	75	85
					Summer				
$K_{yy}(10^{10}\text{cm}^2/\text{s})$	0. 90	1. 16	1. 41	1. 45	1. 25	0. 91	0. 61	0. 48	0. 45
$K_{yz}(10^6\text{cm}^2/\text{s})$	−1. 21	−1. 78	−3. 73	−7. 33	−8. 41	−5. 36	−2. 48	−1. 13	−0. 68
$K_{zz}(10^3\text{cm}^2/\text{s})$	1. 58	2. 00	3. 21	6. 51	7. 73	5. 38	2. 83	1. 16	0. 80
					Winter				
$K_{yy}(10^{10}\text{cm}^2/\text{s})$	1. 17	1. 46	1. 86	2. 35	3. 33	4. 46	5. 50	6. 25	6. 20
$K_{yz}(10^6\text{cm}^2/\text{s})$	−3. 48	−5. 28	−10. 39	−14. 36	−15. 91	−16. 75	−15. 33	−11. 31	−8. 05
$K_{zz}(10^3\text{cm}^2/\text{s})$	2. 68	3. 96	8. 96	12. 53	12. 41	11. 51	10. 20	8. 56	7. 08
					Spring				
$K_{yy}(10^{10}\text{cm}^2/\text{s})$	0. 77	0. 90	1. 02	1. 23	1. 35	1. 28	1. 17	1. 02	0. 87
$K_{yz}(10^6\text{cm}^2/\text{s})$	−2. 13	−2. 80	−5. 00	−7. 85	−8. 38	−7. 38	−5. 62	−1. 32	1. 47
$K_{zz}(10^3\text{cm}^2/\text{s})$	1. 73	2. 22	4. 18	7. 25	7. 67	6. 27	4. 50	2. 23	1. 47
					Fall				
$K_{yy}(10^{10}\text{cm}^2/\text{s})$	1. 43	1. 67	2. 15	2. 57	2. 93	3. 68	4. 12	3. 00	1. 96
$K_{yz}(10^6\text{cm}^2/\text{s})$	−2. 83	−3. 78	−7. 92	−12. 98	−14. 72	−11. 52	2. 35	12. 87	12. 60
$K_{zz}(10^3\text{cm}^2/\text{s})$	2. 57	3. 22	6. 73	11. 80	13. 03	10. 07	8. 83	10. 57	11. 50

meteorological transports may not play a significant role in determining the ozone distribution in those regions due to short photochemical regeneration times. Such transports could be important at high latitudes in the winter, however.

Time-Zonal Mean State of the Model Stratosphere Under the Influence of Transport and Radiative-Photochemical Effects

The meridional cross sections for summer and winter seasons representing the zonal mean temperature, ozone mixing ratio, and zonal wind as computed for the case 2 experiment are shown in figures 5, 6, and 7, respectively. The flow pattern resulting from the individual velocity components of the mean meridional motions is illustrated in figure 8. The flow pattern was obtained by computing the stream function that satisfies the equation of continuity in the meridional plane.

The computed distributions show several features more representative of the observed distributions than the radiative-photochemical equilibrium model. Let us consider the changes that took place in the temperature structure and in the distributions of the ozone mixing ratio from case 1.

We note that in the lower stratosphere the incorporation of the transport processes resulted in a dramatic reversal of the latitudinal temperature and ozone mixing ratio gradient in the case 2 experiment, with temperature and ozone mixing ratio values increasing from low to high latitudes (figs. 5, 6). In the winter lower stratosphere, for example, the temperature has increased about 10°K from the Tropics to high latitudes, and the ozone mixing ratio has increased by a factor of 2 on the average. Both features are consistent with the measured values in the lower stratosphere, and they represent a significant improvement on the results of the case 1 experiment. We also note in figure 5 that the tropopause was indicated at about 16 km in the Tropics and around 13 km in polar latitudes, which is also consistent with the observations. Note, however, that the temperature structure in the winter lower stratosphere (fig. 5) does not indicate the observed midlatitude warm belt with cold temperatures at the pole. Calculations on a gridpoint basis, however, show the highest temperatures around 50°N and a slight decrease of temperature toward the pole. As can be seen later, this feature is more evident in case 4 results, when vertical variation is introduced in the diffusion coefficients.

It is important to mention at this point that the preliminary experiments with Fickian diffusion have not resulted in any significant increase of temperature and ozone with latitude in the lower stratosphere, showing that the large-scale, quasi-horizontal eddy mixing on a sloping surface is mainly responsible for the above events.

The temperature and ozone changes in the middle and upper stratosphere are small at all latitudes in summer and small in the Tropics during the winter season. The close comparison between cases 1 and 2 experimental results in the summer upper stratosphere shows that the transport processes are less important. In the winter high latitudes, however, the changes from case 1 are quite

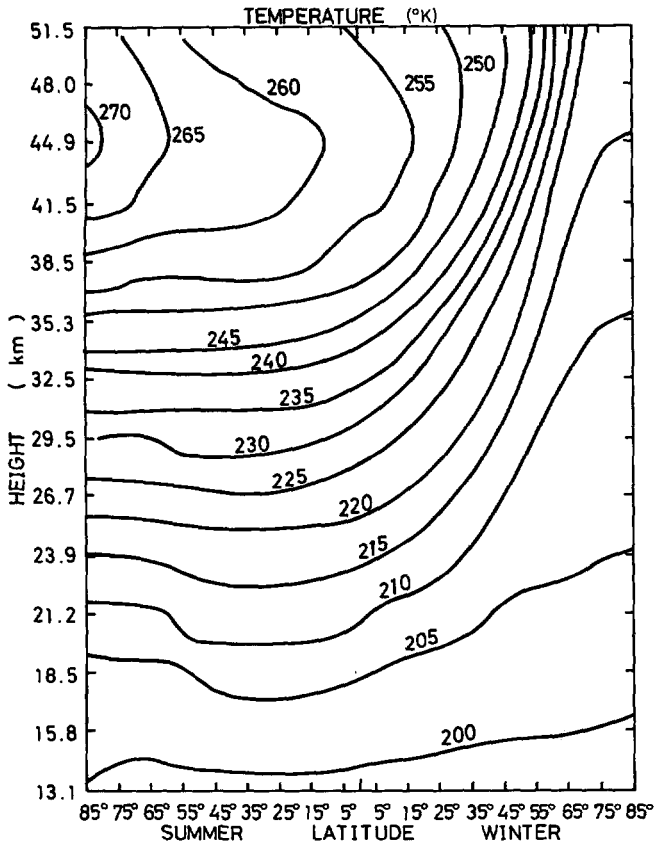

FIGURE 2.—Meridional cross section of temperature for the radiative-photochemical equilibrium state of case 1.

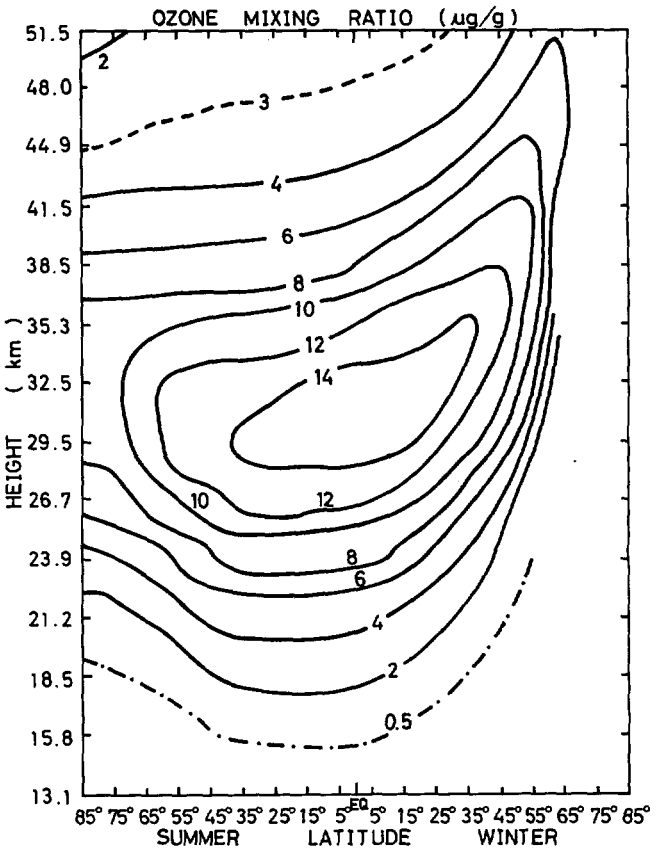

FIGURE 3.—Meridional cross section of ozone mixing ratio (µg/g) for the radiative-photochemical equilibrium state of case 1.

significant, and values in case 2 compare favorably with observations. For example, the computed temperatures around 250°K at 50 km in the subpolar regions during the winter season correspond well with the observed values given by Murgatroyd et al. (1965). Furthermore, the northward transports of heat against the dissipative effects of long-wave radiation in winter high latitudes have resulted in the formation of the stratopause (fig. 5) although not well marked. We also note rather high values of ozone mixing ratio in the winter polar regions (fig. 6), which may account for the observations in those regions. In view of the fact that there was no production of ozone in the winter polar regions, these high values of ozone mixing ratio can only be brought about by the meteorological transports in our model from the production regions.

Despite the good overall agreement in the main features between computed temperature and ozone distributions in case 2 and observations, there are differences in detail. In the case of ozone, we will highlight these differences, which are not readily discernable in the meridional cross-section presentation, by comparison of vertical profiles at specific latitudes for winter in figure 9. We note that the computed values of ozone mixing ratio were consistently overestimated at all latitudes near the level of ozone maximum. This is also true to a lesser extent in the lower stratosphere except in the high latitudes where the computed values were slightly less than the observations.

In figure 10, the latitudinal distributions of total ozone computed in cases 1 and 2 experiments are compared

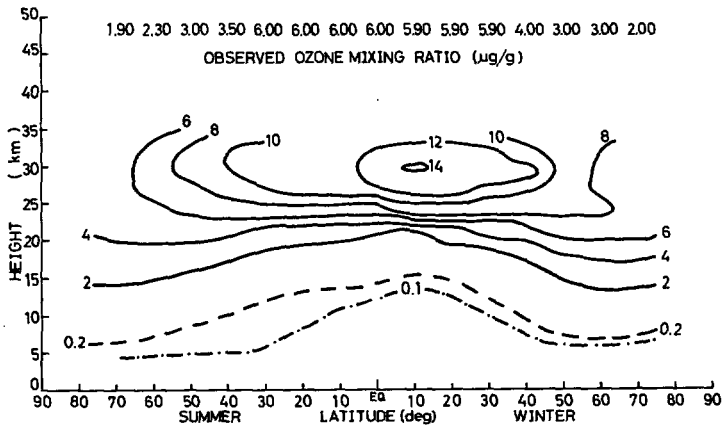

FIGURE 4.—Meridional cross section of observed ozone mixing ratio in summer and winter. The distribution is based on bi-monthly means of North American ozone-sonde data compiled by Hering and Borden (1964).

with the observed amounts for the summer and winter seasons. The latitudinal distribution of total ozone computed from the case 3 experiment, which will be discussed later, is also shown in figure 10. It is clear from figure 10 that the modeled transports and their interactions with the radiative-photochemical effects in the case 2 experiment brought the latitudinal distribution of total ozone into good agreement with the observed total amounts. However, as indicated by the vertical profiles (fig. 9), the computed total amounts in the case 2 experiment were overestimated in both hemispheres, except in high latitudes during the summer. The transport processes,

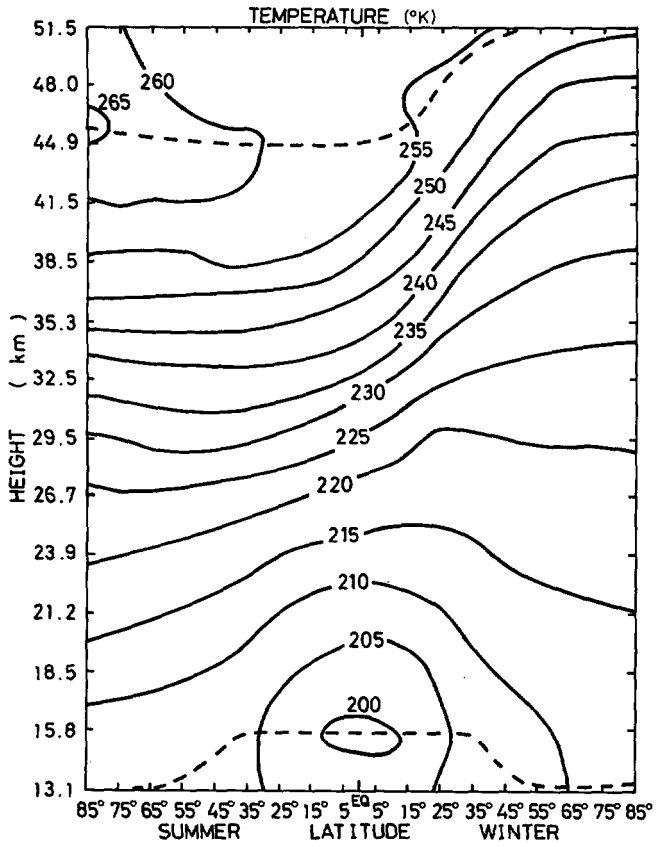

FIGURE 5.—Steady-state distribution of temperature (°K) in the meridional plane for summer and winter from the case 2 experiment. The tropopause and stratopause are indicated by dashed lines.

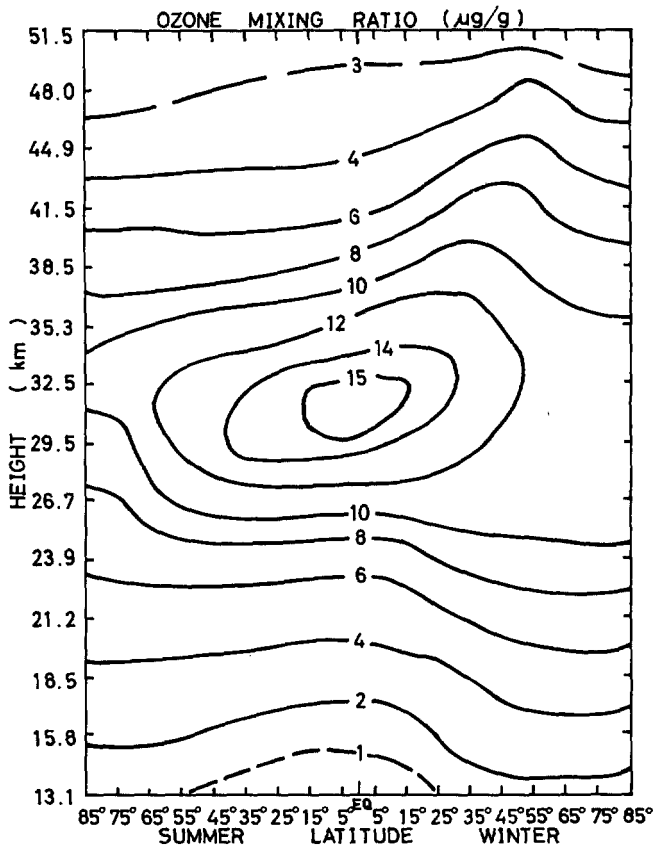

FIGURE 6.—Steady-state distribution of ozone mixing ratio in the meridional plane for summer and winter from case 2 experiment.

as modeled, appear to result in excessive flow of ozone northward near the level of ozone maximum, especially in winter, which in turn produces higher values of ozone mixing ratio and consequently higher total amounts than observed. We note from the zonal wind cross section (fig. 7) that the significant observed features such as the jetlike strong westerlies in the subtropical winter season and the strong easterlies in the tropical regions in summer are reproduced reasonably well by the model computations. Incursion of the summer easterlies into the tropical winter below 35 km is consistent with the observations and is probably caused by the interhemispheric transports. The weak midlatitude westerlies in the summer upper stratosphere do not agree with the observations. The lack of vertical structure in the diffusion coefficients in case 2 apparently contributed to the poor horizontal temperature structure, resulting in the unrealistic zonal winds in that region.

Another feature that is not consistent with the observations is the marked discontinuity in the zonal wind field across the Equator in the upper stratosphere. This is a result of the thermal wind approximation, which is not a good one in the Tropics.

The mean meridional circulation developed in the model has a two-cell structure in the winter lower stratosphere (fig. 8) with, generally, a rising motion in the Tropics and in the subpolar and polar regions with subsidence flow in the subtropics and middle latitudes. The flow

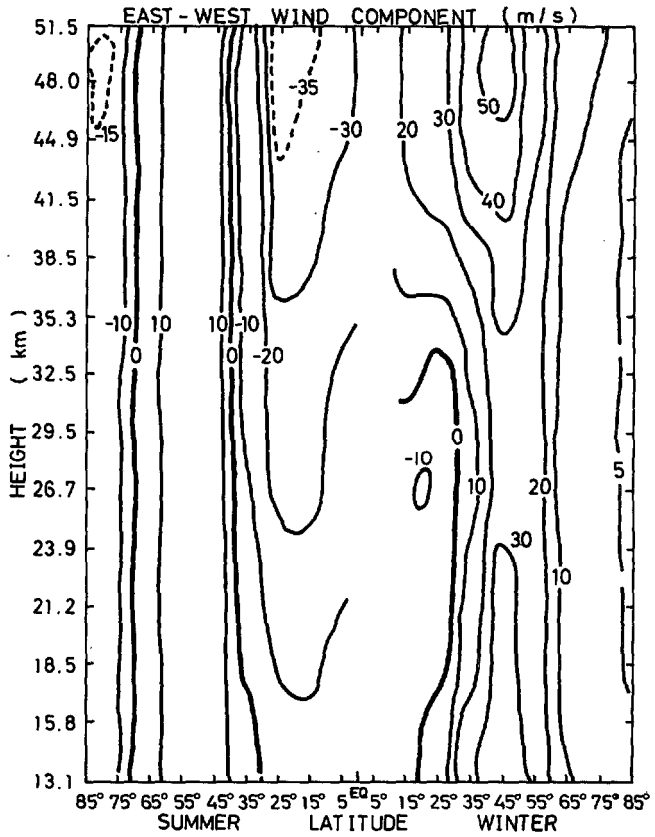

FIGURE 7.—Meridonal cross section of the time-zonally averaged east-west, $\bar{u}$, wind component for summer and winter from case 2 experiment. Negative values represent easterlies.

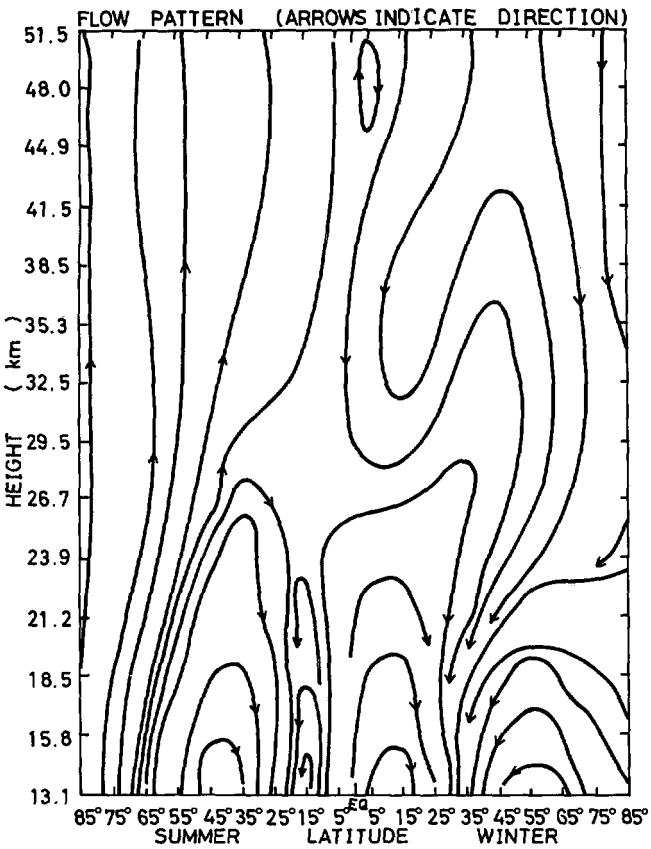

FIGURE 8.—The flow pattern of the mean meridional circulation for summer and winter from the case 2 experiment.

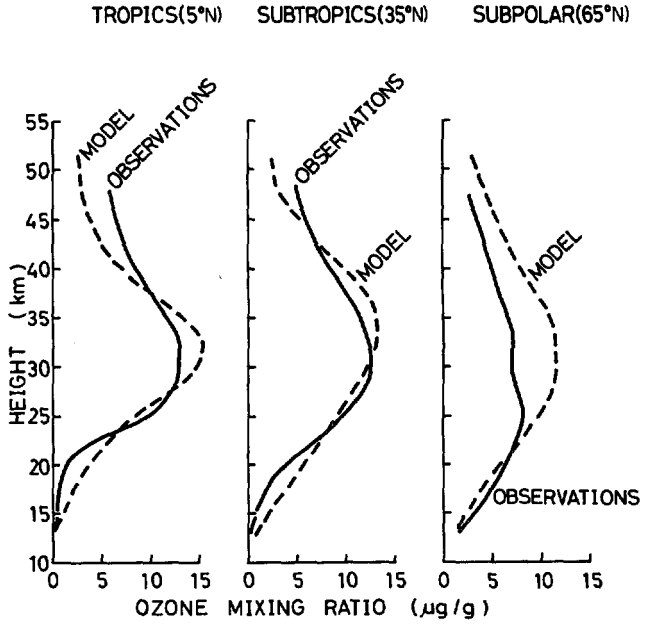

FIGURE 9.—Vertical distribution of ozone mixing ratio in case 2 at selected latitudes compared with the mean observations of Hering and Borden (1964) for winter season.

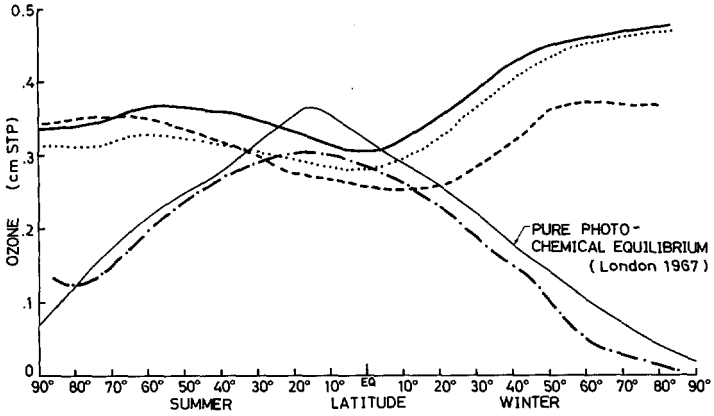

FIGURE 10.—Comparison of the equilibrium distribution of total ozone from case 1 (dash-dot line) and the final equilibrium distribution of total ozone computed from case 2 (heavy solid line) with the observed total amounts (dashed line) as given by Prabhakara (1963) for summer and winter seasons. Also shown for comparison are the pure photochemical equilibrium results of London (1967) and final equilibrium results of case 3 (dotted line).

pattern for the summer lower stratosphere is similar to that during the winter season except that the whole pattern is shifted toward the Equator.

The computed circulation pattern in the lower stratosphere, shown in figure 8, corresponds closely with the indirect computation of the mean meridionial flow based on observed information (Teweles 1964, Vincent 1968). Also, the magnitudes of the vertical motions in the lower stratosphere of our model are generally within the range of the observed values.

Manabe and Hunt (1968) also calculated mean meridional motions for the winter stratosphere. Their circulations are similar to that shown in figure 8 for the lower stratosphere except the vertical extent of their winter polar cell was greater. Differences in the results can be attributed to the seasonal lag and the lack of vertical structure in the diffusion coefficients in the case 2 results, in addition to the basic differences in the two models.

The flow pattern in the middle and upper stratosphere during the winter season indicates upward motion in the subtropical regions with the compensating downward motions on either side of it. In summer, however, the flow is generally upward.

Seasonal Transport and Physical Mechanisms

To assess the relative importance of various physical and transport processes operating in the stratosphere, we evaluated the budgets of heat and ozone using the case 2 experimental results.

Heat budget. In figure 11, the variation of various heat balance components with latitude are shown at two levels representing the lower and upper stratosphere. The principal components contributing to the heat budget are the large-scale quasi-horizontal eddy effects, the vertical component of the mean meridional motion, and the net radiation in both the lower and upper stratosphere, and for the summer and winter seasons. Note that in the lower stratosphere the large-scale eddy processes are transporting more heat from the Tropics and subtropics to middle and high latitudes than is required to compensate for the

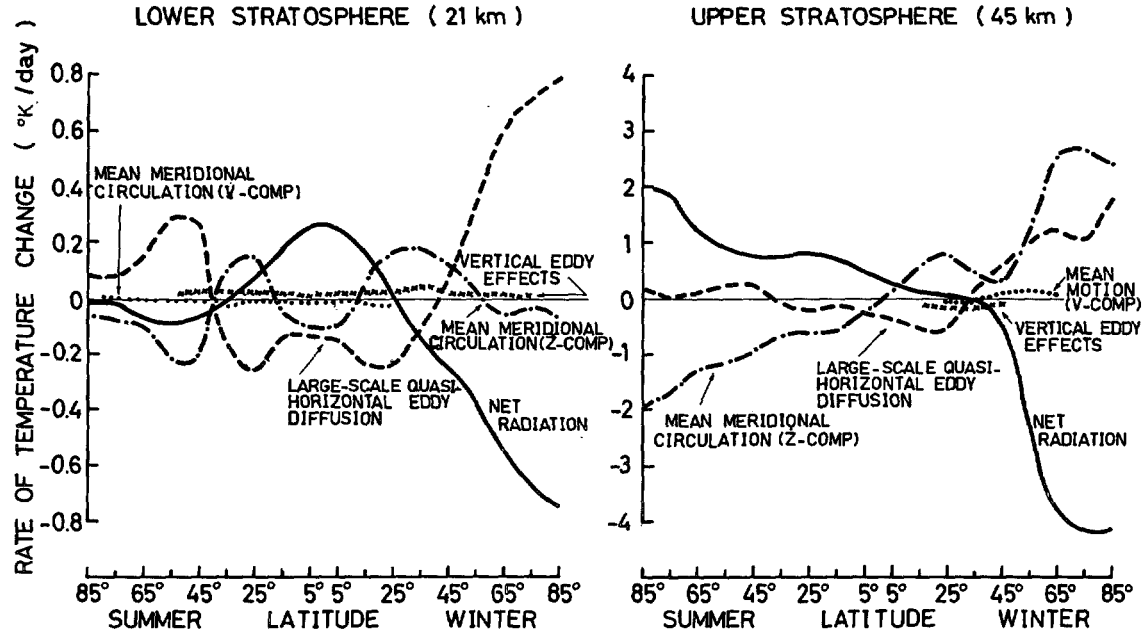

FIGURE 11.—The latitudinal variation of the various heat balance components (deg/day) in the lower and upper stratosphere for summer and winter from case 2.

radiational heat deficit. On the other hand, the excess heat from the Tropics (generated by radiation) and from high latitudes was removed by the vertical component of the meridional circulation, which is simultaneously supplying heat to the subtropics. Although there is negligible contribution from the north-south component of the mean meridional motion, it is not appropriate to separate its budget effects from the vertical component because of the complete balance between two components in the equation of continuity.

Relatively little information is available on heat transports from observed data, particularly in the middle and upper stratosphere. However, the results of the model with regard to heat transports by the large-scale, quasi-horizontal eddy effects in the lower stratosphere agree in a qualitative sense with the observed estimates by Oort (1963) of transient heat fluxes.

Manabe and Hunt (1968) have also made heat balance calculations of the winter stratosphere from the general circulation model. Exact comparison between the two results is not possible. However, the heat balance components they have computed at 25 km agree approximately in both magnitude and sign with the results shown in figure 11 for the winter stratosphere except that the strength of the mean meridional circulation, and therefore the magnitude of its contribution to the heat balance, was underestimated in the case 2 results.

Ozone budget. Although the predominant balance in ozone is between the large-scale, quasi-horizontal eddy effects and the contribution from the vertical component of the mean meridional motions, the contributions of vertical eddy effects and the north-south component of the mean motion are important for complete balance.

The relative roles of various mechanisms in the maintenance of ozone are illustrated in figure 12, as a function of latitude, at two representative levels of the lower and upper stratosphere, respectively. Contrary to the classical view (Brewer 1949) that the late winter and spring build-up in the high latitude lower stratosphere is attributable to transport by the mean meridional cell, this model demonstrates that the ozone transports to high latitudes are mainly due to large-scale eddy fluxes. The vertical eddy effects played a substantial role in the winter high latitudes in balancing the northward transports of ozone by the quasi-horizontal eddies. The main function of the mean meridional motions in the two hemispheres is apparently to remove the ozone tracer from the Tropics and high latitudes, and deposit it in the subtropical regions. On the other hand, the quasi-horizontal eddies transport ozone northward into high latitudes mainly from this subtropical area of concentration. However, more ozone was transported to high latitudes by the horizontal eddy effects than was removed by the vertical component of the mean motion, and the excess was balanced by downward transports due to vertical eddies in winter and by the photochemical sink in summer in high latitudes. In the Tropics, the ozone removed by the vertical component of the mean motion was replaced partly by the photochemistry and partly by ozone convergence due to horizontal eddy effects, which might have been caused by the interhemispheric transports.

In the winter upper stratosphere, the main source of ozone production was located in middle latitudes, probably due to the inverse temperature effect on the photochemical production of ozone that was so evident in the case 1 results. From this source, the quasi-horizontal eddy processes transported ozone both northward and southward (predominantly northward) to fill the photochemical sinks in those regions. Again, in the winter high latitudes, the excess ozone transported by the horizontal eddy pro-

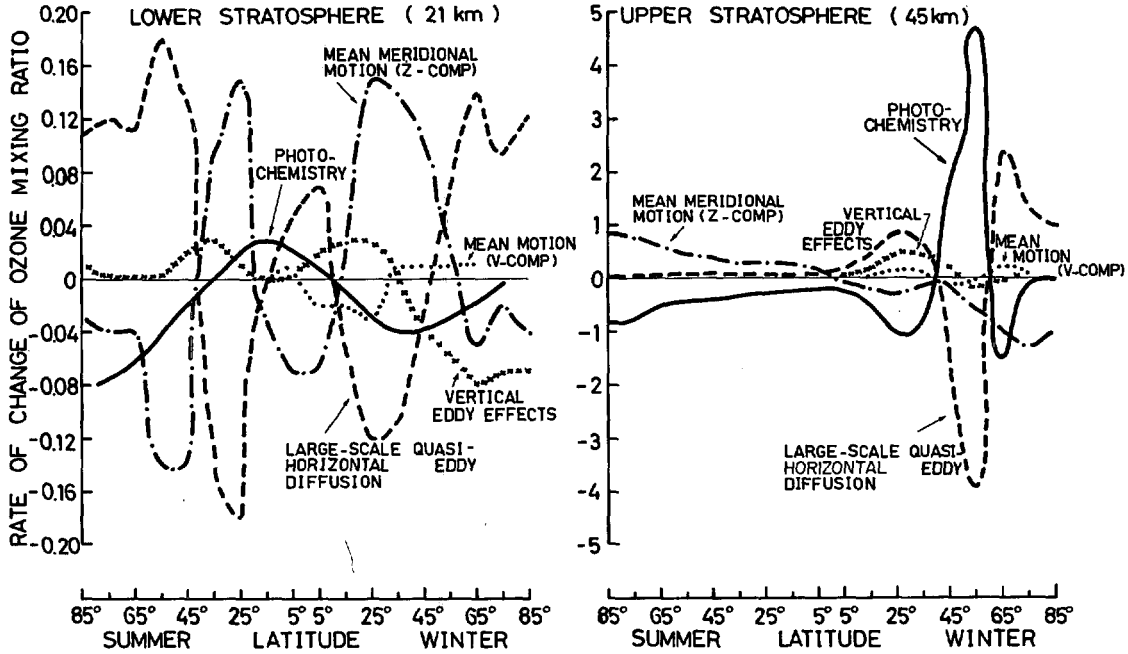

FIGURE 12.—The latitudinal variations of various balance contributions to the ozone budget ($10^{-1}\mu g \cdot g^{-1} \cdot day^{-1}$) in the lower and upper stratosphere from case 2.

cesses over the photochemical sink was balanced by ozone removal due to the vertical component of the mean motion. In the subtropical winter, apart from the mutual opposition between photochemistry and horizontal eddy processes, the vertical eddy effects and the contribution from the north–south component of the mean motion roughly balance each other. In the summer upper stratosphere, however, both horizontal and vertical eddy effects were weak in the model; therefore, the photochemical sinks in that region were mainly balanced by the contributions from the vertical component of the mean motion.

The relative importance of the radiative-photochemical and transport processes depends on their relative time scales (characteristic times). It appears that, due to small characteristic times for radiative-photochemical processes, the transport processes have relatively small effect on the distribution of ozone or temperature in the summer upper stratosphere.

Results of the Case 3 Experiment

The linear constraint on the thermodynamic energy source was removed in the case 3 experiment by incorporating detailed calculations for the long-wave radiation transfer based on physical considerations. The diffusion coefficients used in this experiment were exactly the same as in case 2 for summer and winter (table 1). The results show that the meridional cross sections of temperature, mean circulation, and ozone are similar to those in case 2 except for small differences in detail. The case 3 experiment for summer and winter produced better temperature gradients than case 2 did in the upper stratosphere but poorer ones in the lower stratosphere. As shown in figure 10, however, improved latitudinal distribution of total ozone occurred in the case 3 experiment. A detailed discussion on case 3 results is given in Rao (1970).

Results of the Case 4 Experiment

One unsatisfactory feature we have noticed in the case 2 (also in case 3) experiment, particularly in the middle latitude summer, was the lack of a realistic vertical structure in the distribution of zonal winds. This deficiency appears to result from a lack of vertical structure in the diffusion coefficients, K_{yy} and K_{yz}, which contributed to insufficient heat transports and horizontal temperature gradients. Therefore, we decided to vary the diffusion coefficients, K_{yy} and K_{yz}, in the vertical dimension as well. The diffusion coefficients for the lower stratosphere were taken as reported by Reed and German; those for the higher levels were derived from Newell's wind statistics. Except for the vertical variation of diffusion coefficients in this experiment, conditions were the same as in case 2. The temperature and zonal wind distributions resulting from this experiment are shown in figures 13 and 14, and the circulation pattern of the mean meridional motions is illustrated in figure 15. Immediately apparent from figure 13 is the appreciable improvement in the horizontal temperature structure in both hemispheres in the lower stratosphere over that derived from the case 2 experiment. For instance, the temperature gradient from the Equator to the pole in summer in the lowest three levels of the model is quite close to the observations. Note also the 15°K increase of temperature from the Equator to a maximum around 55°N with lower temperatures farther north in the winter lower stratosphere, roughly in agreement with the observations. In the middle and upper stratosphere, however, the changes are slight; there is, however, a better indication of the stratopause formation in the winter high latitudes.

Associated with the improved horizontal temperature structure in the lower stratosphere, is a much improved vertical structure of the zonal wind distribution, especially

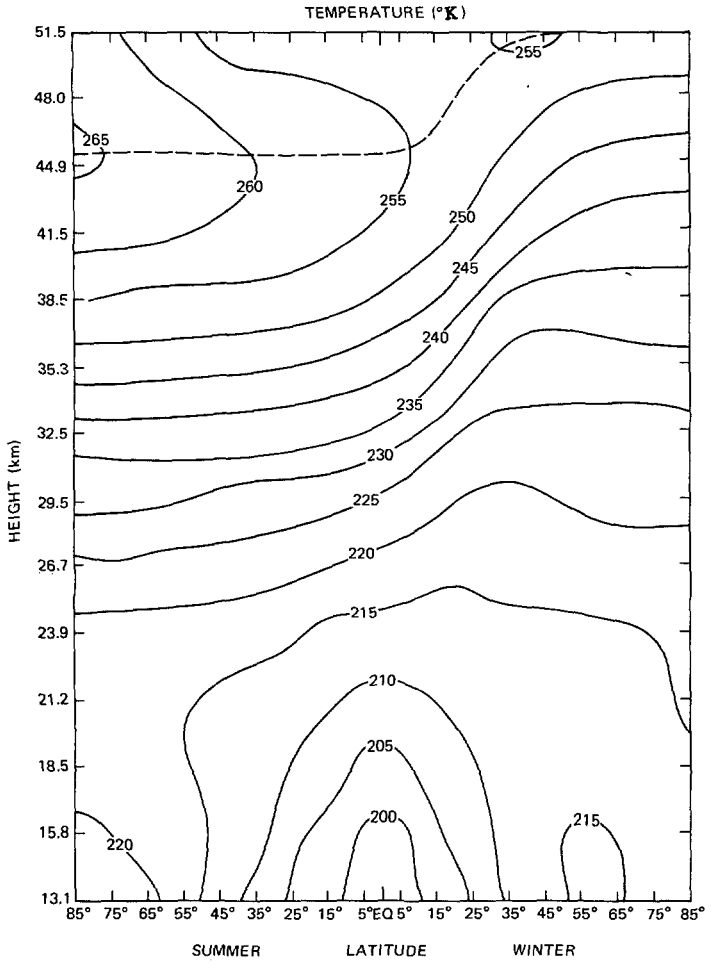

FIGURE 13.—The steady state distribution of temperature in the meridional plane for summer and winter in case 4. The stratopause is indicated by the dashed line.

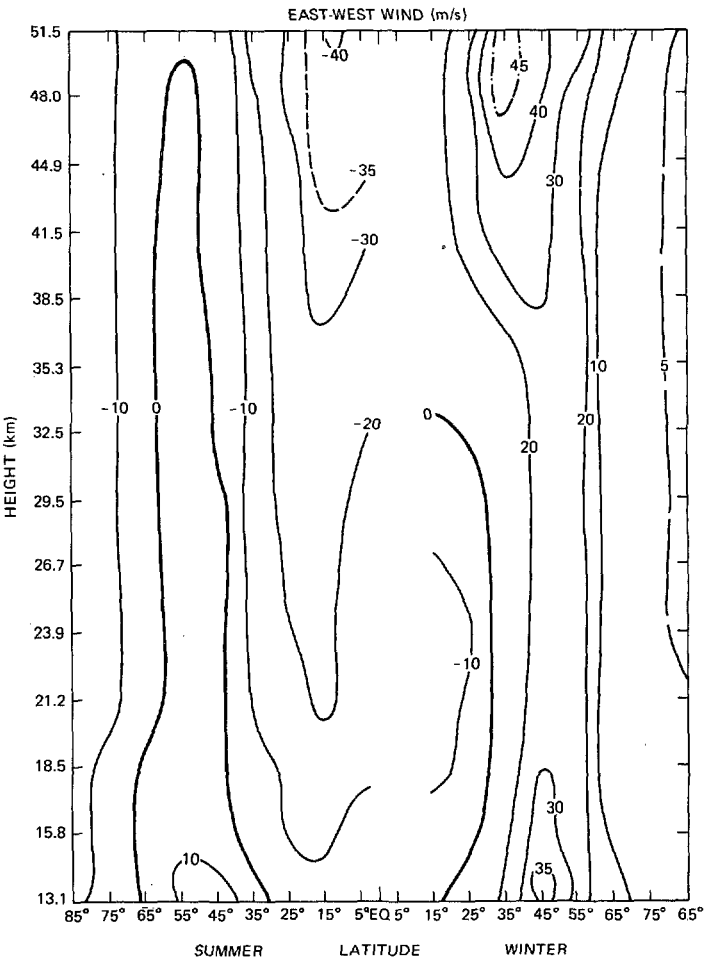

FIGURE 14.—The meridional cross section of time-zonal mean east-west wind component, $\bar{u}$, for summer and winter in case 4.

in the middle latitude summer (fig. 14). For example, the specified zonal winds of 17–18 m/s in the middle latitude summer were reduced to zero and slight easterlies in the upper stratosphere. This confirms the idea that the poor zonal wind structure in the middle latitude summer was *partly* due to lack of vertical structure in the diffusion coefficients in case 2; the results, however, still do not agree with the observed easterlies, which require even stronger horizontal temperature gradients.

The circulation pattern of the mean meridional motions for case 4 (fig. 15) shows a much greater resolution in the two-cell structure in the summer lower stratosphere than that for case 2. In addition, the vertical extent and the strength of the high latitude cell in the winter lower stratosphere are in better agreement with the results of Manabe and Hunt (1968).

The meridional cross section of ozone in case 4 was similar to that in case 2 and, therefore, it is not necessary to present it here. However, it should be mentioned that the total ozone amounts were higher in case 4 because of stronger northward ozone transports by the quasi-horizontal eddy processes in the lower stratosphere. It appears that the diffusion coefficients based on heat transport data were a little too strong for the ozone transports in the model.

The Boundary Conditions

To test the effect of lower boundary condition on temperature, we reduced the lower boundary temperatures for summer and winter by 5 percent, a change of 10°–12°K at each latitude, and the case 2 experiment was repeated with the new conditions. The results show that modification of lower boundary temperatures has no influence on the distribution of temperature within the model region except for some minor changes at the lowest two levels near the lower boundary. When the upper boundary temperatures were also changed by 5 percent, the changes that resulted near the upper boundary were even less significant. The lack of response of the interior temperature field to these boundary changes is probably due in part to the lack of significant vertical heat transports within the model.

The effects of changes in the ozone mixing ratio at the lower boundary on the interior distribution of ozone were also tested by deliberately minimizing ozone mixing ratio values at the lower boundary. Altering the lower boundary mixing ratio values by a factor of 2–3, depending upon the latitude, alters the total ozone amounts by about 10 percent; there is an indication that this change is due to downward transport of ozone by vertical eddy processes

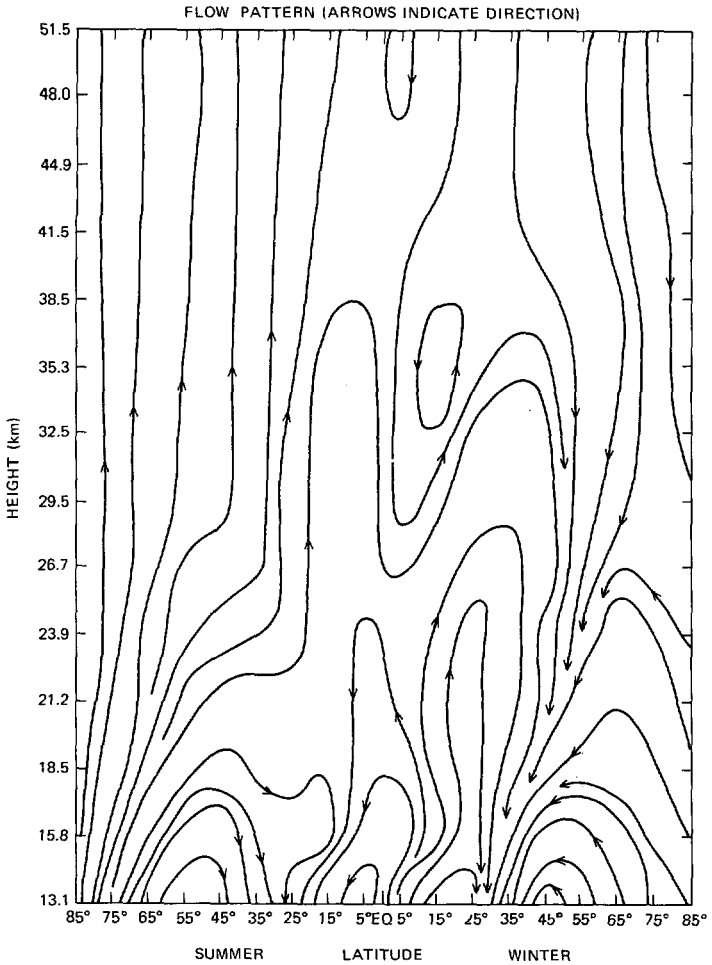

FIGURE 15.—The flow pattern of the mean meridional circulation for summer and winter in case 4.

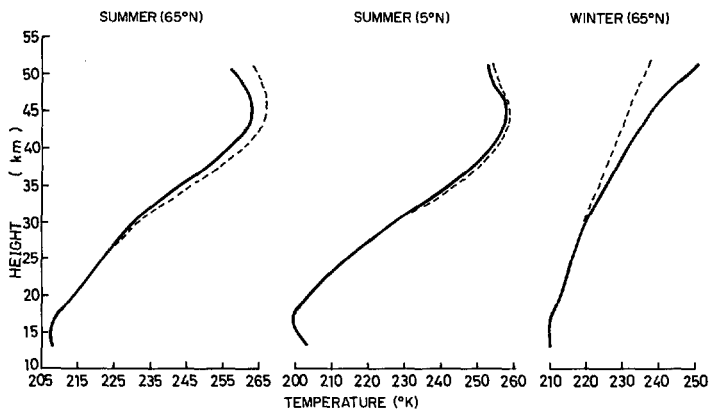

FIGURE 16.—Influence of the modified vertical velocities at the upper boundary on the vertical distribution of temperature at selected latitudes. The dashed curves represent the zero vertical velocity specification at the top (i.e., the modified boundary).

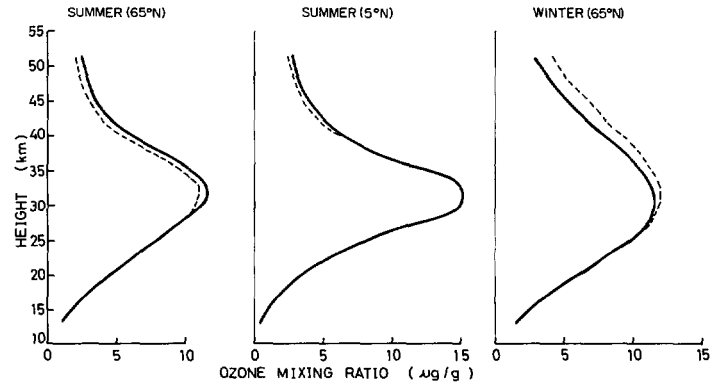

FIGURE 17.—Influence of the modified vertical velocities at the upper boundary on the vertical distribution of ozone mixing ratio at selected latitudes. The dashed curves represent the zero vertical velocity specification at the top (i.e., the modified boundary).

in the model when strong vertical gradients of the ozone mixing ratio were imposed at the lower boundary.

The vertical velocities specified at the top boundary of the model for this study are based on the approximate balance between the static stability term and net radiation in the thermodynamic energy equation and were taken from Murgatroyd and Singleton (1961). Because there is some doubt as to the validity of these values in the winter high latitudes, we decided to test a specification of zero vertical velocities at the top by making $\dot{Z}=0$ everywhere at the top boundary. This is an extreme condition, and it is unlikely to represent a true situation in the real atmosphere at that level. The vertical profiles of temperature and ozone mixing ratio corresponding to the two sets of boundary conditions are compared in figures 16 and 17 at 65°N and 5°N in summer and at 65°N in winter. Comparison of the two temperature profiles at 65°N in winter with the observations shows that the zero vertical velocity condition at the upper boundary is quite unrealistic. For instance, the temperatures corresponding to the dashed curve (representing $\dot{Z}=0$ at the top) are 10°–13°K lower than the observed, while the solid curve (with nonzero vertical velocities at the top) agrees well with observations. This suggests that the top boundary specification of the vertical velocities in winter high latitudes is a reasonable condition. The ozone changes caused by the variation of vertical velocities at the top are not particularly significant, although they are noticeable (fig. 17).

Case 2 and 3 Experiments For Spring and Fall Seasons

For a detailed discussion of the results (including case 3), the reader is referred to Rao (1970). Here we present and discuss briefly only the results of the case 2 experiment. The results are shown in figures 18–20 with the flow pattern for the mean meridional motions illustrated in figure 21.

The temperature distribution in the lower stratosphere fall (fig. 18) shows a pronounced temperature maximum around 55°N from which the temperature decreases toward both the Equator and the pole. In the spring lower stratosphere, however, the temperature maximum has shifted farther to the north and is located around 75° to 80°N.

In the middle and upper stratosphere (fig. 18), the strongest horizontal temperature gradients are found in

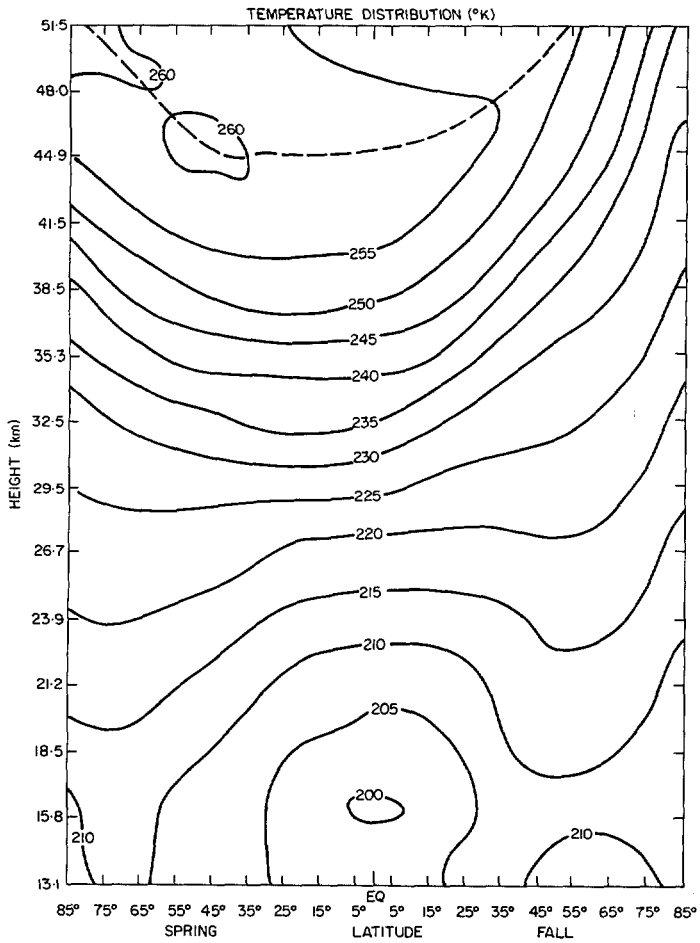

FIGURE 18.—The steady-state distribution of temperature in the meridional plane for spring and fall in case 2. The stratopause is indicated by the dashed line.

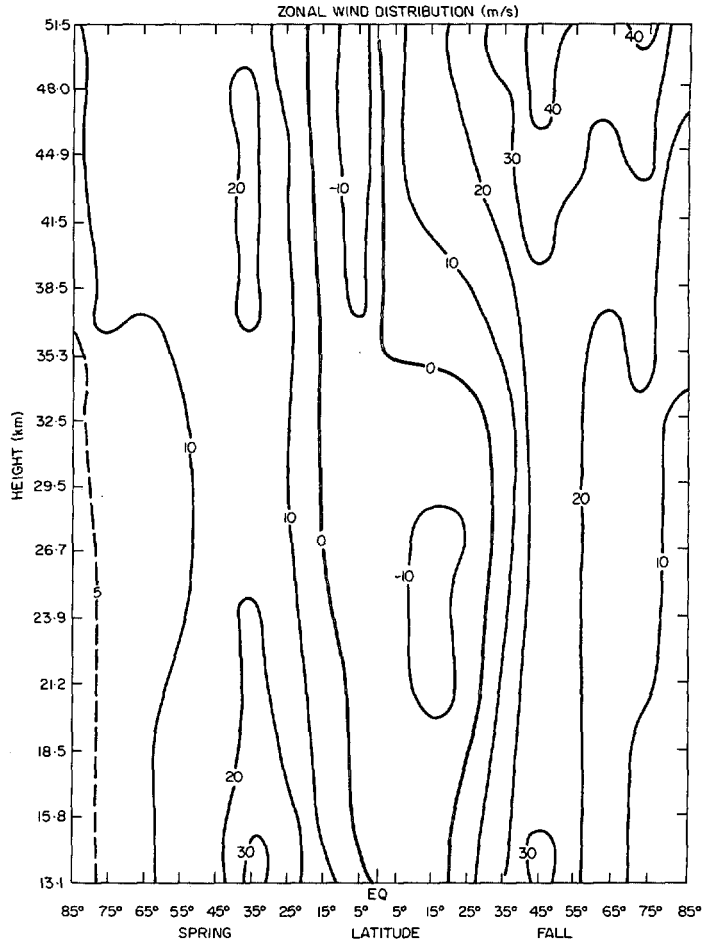

FIGURE 19.—The meridional cross section of time-zonal mean east–west component, $\overline{u}$, for spring and fall in case 2. Negative values represent easterly winds.

middle and high latitudes in both hemispheres, in contrast to the strong gradients that were shown in tropical and subtropical regions in summer and winter in case 2. Note that the temperatures are higher in the Tropics, steadily decreasing toward both poles except at about 45 km in spring, where the temperature gradient is reveresd.

The zonal wind distributions for spring and fall (fig. 19) generally follow the horizontal temperature structure except for the lower boundary effects. Therefore, comments are not necessary except to mention that the double wind maximum of westerlies in the upper stratosphere and the tropical easterlies in the lower levels during the fall season seem to correspond to the early winter conditions in the real atmosphere.

In the cross section of ozone mixing ratio in the lower stratosphere (fig. 20), we see that the model distribution is roughly symmetrical with respect to the two seasons. The stronger diffusion coefficients that correspond to the early winter conditions appear to be too strong for the fall season. The distribution of ozone near the level of ozone maximum and above is similar to that in summer and winter in case 2.

Figure 22 shows the comparison between the computed latitudinal distribution of total ozone and the observed amounts, with the solid and dashed curves representing observed and computed amounts, respectively. Also shown in figure 22 is the latitudinal distribution of total ozone computed from the case 3 experiment for spring and fall, which is represented by the dotted curve. The computed amounts are obviously overestimated at most cf the latitudes, although the spring maximum in the high latitudes is computed correctly. As expected from the meridional distribution of the ozone, mixing ratio in the lower stratosphere, the computed amounts are at least 25 percent higher than the observed in the fall season; in spring, the percentage error is much less, especially in the high latitudes.

From the flow pattern of mean meridional circulations for spring and fall (fig. 21), we see that the three circulation cells in the lower stratosphere during the fall season look like the direct extension of the upper tropospheric cells during the early winter conditions. As a result of the shift of temperature maximum northward near the pole in the spring lower stratosphere, the polar cell almost disappears, resulting in a two-cell structure. During the fall, the middle and upper stratosphere flow is upward in subtropical and middle latitudes with compensating downward motion on either side in a manner similar to that during the winter in case 2. In spring, however, the motion is upward from the Tropics to 55°N in the middle stratosphere with downward motion in the high latitudes; this

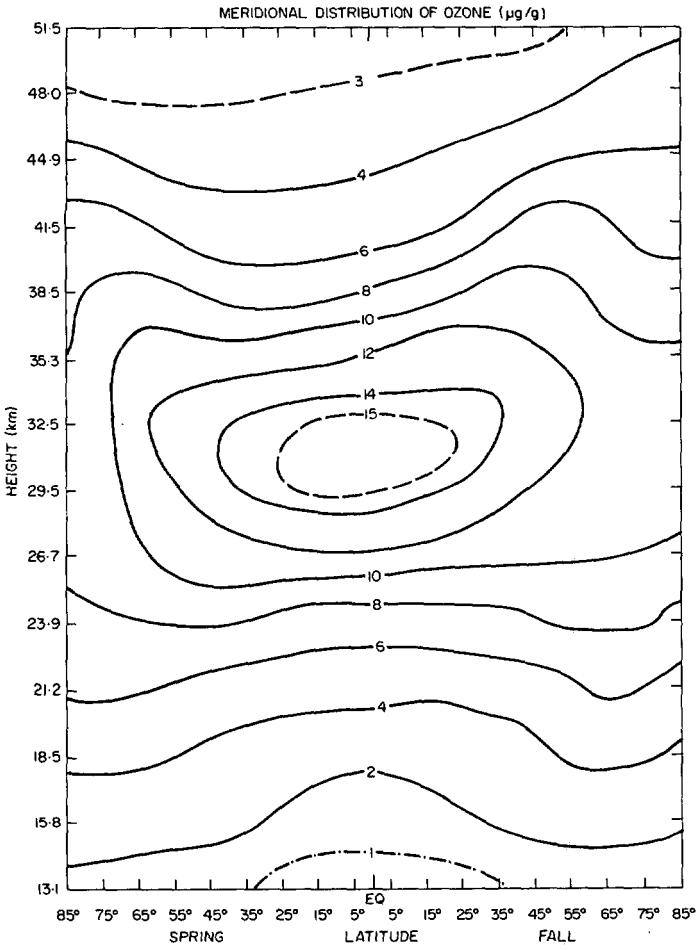

FIGURE 20.—The steady-state distribution of ozone mixing ratio in the meridional plane for spring and fall in case 2.

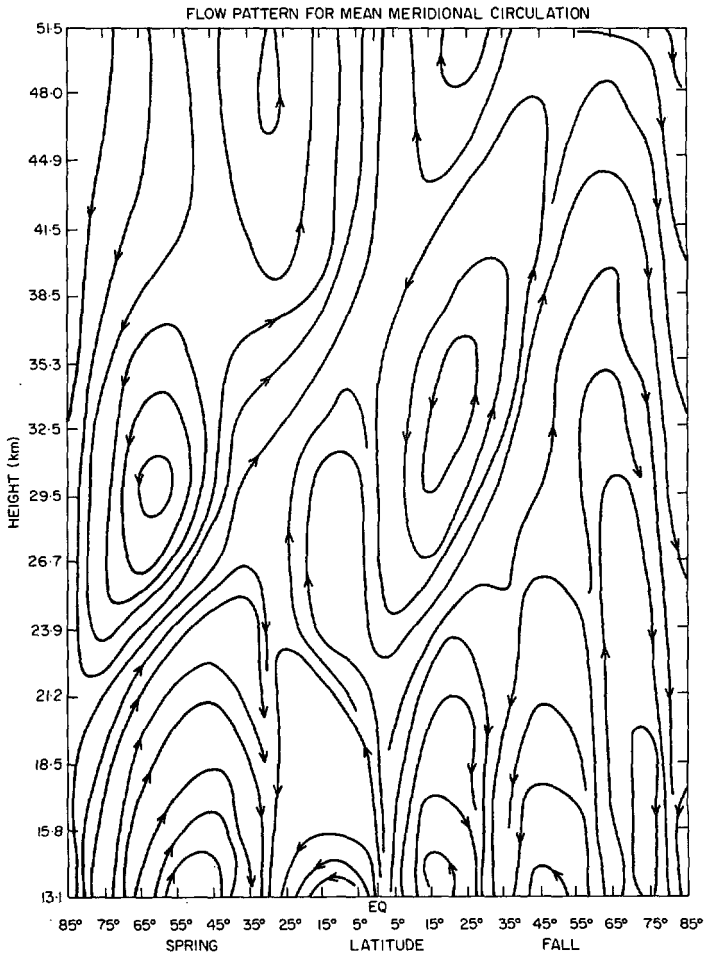

FIGURE 21.—The flow pattern of the mean meridional motions for spring and fall in case 2. Arrows indicate direction.

flow pattern shifts towards the Equator in the upper stratosphere.

To provide a general survey and to conclude the discussion of experimental results, we compare (fig. 23) the latitudinal distributions of total ozone resulting from the various numerical experiments (including the present experiment) with the observed total ozone curve from Prabhakara (1963) for the winter season. Figure 23 shows that the relative performance of various models, either steady state or time-dependent, cannot be judged from the latitudinal distributions of total ozone alone. A clear example of this is given by the results of Hunt (1969), which provide much information on the transport mechanisms involved in the maintenance of ozone distribution in the winter lower stratosphere while having the least agreement with the observed total amounts. Although the agreement between the total ozone curve computed from the present model and the observations is not satisfactory, we have contributed significantly to the understanding of transport mechanisms responsible for the maintenance of the seasonal distributions of various properties in the stratosphere.

7. CONCLUSIONS

Despite the limitations of the model with regard to the eddy processes, a number of interesting conclusions can be

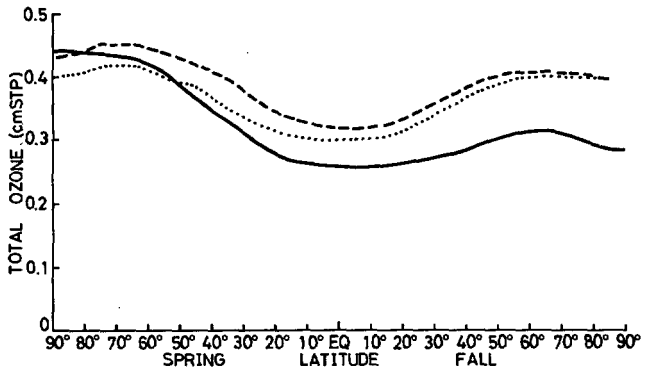

FIGURE 22.—Comparison of the latitudinal distribution of total ozone computed for spring and fall in case 2 (dashed line) with the observed distribution (solid line) taken from Prabhakara (1963). Also shown for comparison is the distribution of total ozone for spring and fall in case 3 (dotted line).

drawn from the comparison of the experimental results with the observations. By comparing case 1 and case 2 results, we find that the modeled transports and their interactions with the physical processes are sufficient to rectify much of the initial discrepancies between the observed and the radiative-photochemical distributions of temperature and ozone in the winter stratosphere and the summer lower stratosphere. In the lower stratosphere, the required heat and ozone were supplied to the sub-

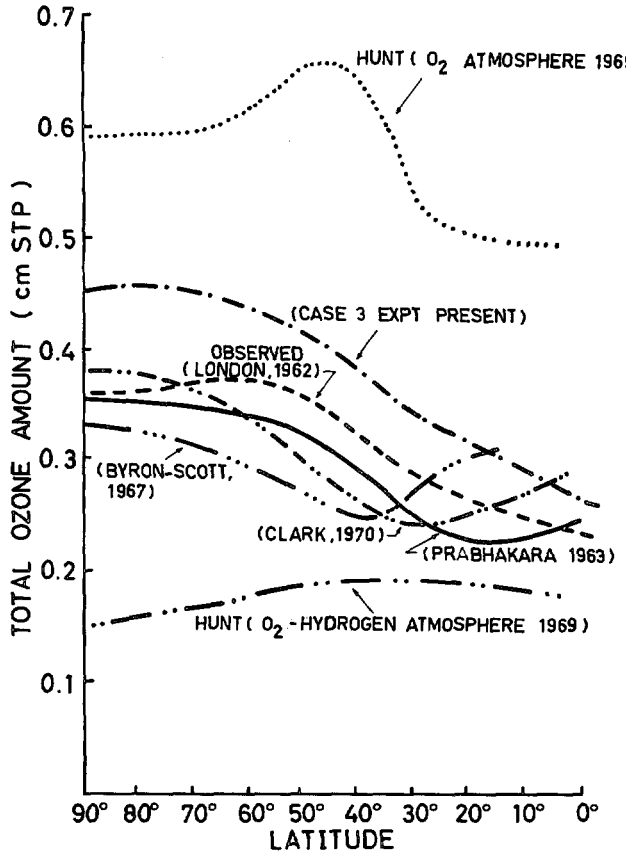

FIGURE 23.—Comparison of the observed latitudinal distribution of total ozone in winter given by Prabhakara (1963) with the results of various time-dependent and steady-state models, including the present model.

tropical regions by the mean meridional motions and then transported northward by the quasi-horizontal eddy effects. At higher levels in the winter stratosphere, the temperatures were maintained by both subsidence and and northward heat transports against the strong long-wave cooling. The high ozone mixing ratio values in the polar regions were mainly due to northward ozone transports by the large-scale eddy processes from the middle latitude photochemical source.

As a consequence of the generalized diffusion in case 2 and later, the mean meridional motions developed the two-cell structure typical of recent observational studies of the winter lower stratosphere. Both quasi-horizontal eddies and mean meridional motions contributed significantly to all three budgets, whereas the vertical eddies had little effect except to transport ozone downward in the winter lower stratosphere.

The results of these experiments reveal the fundamental role played by the mean meridional motions and the large-scale, quasi-horizontal eddy effects, especially the latter, in the maintenance of the seasonal distributions in the stratosphere, in the presence of the physical processes, and constitute a valuable contribution to the general understanding of the seasonal climatology of the stratosphere.

Future extensions of this work should give more emphasis to the two-dimensional distribution of the diffusion coefficients and should try to avoid the thermal wind constraint.

ACKNOWLEDGMENTS

The author is grateful to B. W. Boville for his encouragement and many helpful suggestions during the course of this investigation, A. D. Christie for critically reviewing the manuscript, and the Atmospheric Environment Service of Canada for support and the approval of this publication.

REFERENCES

Brewer, A. W., "Evidence for a World Circulation Provided by the Measurements of Helium and Water Vapour Distribution in the Stratosphere," *Quarterly Journal of the Royal Meteorological Society*, Vol. 75, No. 326, London, England, Oct. **1949**, pp. 351–363.

Brewer, A. W., "The Rate of Production of Ozone in the Lower Stratosphere," *Publication in Meteorology* No. 80, Arctic Metorology Research Group, Department of Meteorology, McGill University, Montreal, Canada, May **1966**, pp. 195–198.

Byron-Scott, R., "A Stratospheric General Circulation Experiment Incorporating Diabatic Heating and Ozone Photochemistry," *Publication in Meteorology* No. 87, Arctic Meteorology Research Group, Department of Meteorology, McGill University, Montreal, Canada, Apr. **1967**, 201 pp.

Chapman, Sydney, "A Theory of Upper-Atmospheric Ozone," *Memoirs of the Royal Meteorological Society*, Vol. 3, No. 26, London, England, June **1930**, pp. 103–125.

Clark, John H., "Infrared Heating Due to Ozone," M.Sc. thesis, Department of Meteorology, McGill University, Montreal, Canada, **1963**, 55 pp.

Clark, John H., "A Quasi-Geostrophic Model of the Winter Stratospheric Circulation," *Monthly Weather Review*, Vol. 98, No. 6, June **1970**, pp. 443–461.

Craig, Richard A., "The Observations and Photochemistry of Atmospheric Ozone and Their Meteorological Significance," *Meteorological Monographs*, Vol. 1, No. 2, American Meteorological Society, Boston, Mass., Sept. **1950**, 50 pp.

Dobson, G. M. B., Harrison, D. N., and Lawrence, J., "Measurements of the Amount of Ozone in the Earth's Atmosphere and Its Relation to Other Geophysical Conditions," *Proceedings of the Royal Society of London*, Ser. A, Part II, Vol. 114, No. 768, England, Apr. **1927**, pp. 521–541.

Dütsch, H. U., "Photochemische Theorie der Atmosphärischen Ozons unter Berucksichtigung von Nichtgleishchgewichtzuständen and Luftbewegungen," Doctoral Dissertation, University of Zurich, Switzerland, **1946**, 113 pp.

Eliassen, A., "The Quasi-Static Equations of Motion With Pressure as Independent Variable," *Geofysiske Publikasjoner*, Vol. 17 No. 3, Norske Videnskaps-Akademi i Oslo, Universitetsforlaget, Oslo, Norway, **1949**, 43 pp.

Hering, W. S., and Borden, T. R., Jr., "Ozonesonde Observations Over North America, Vol. 2," *Environmental Research Papers* No. 38, U.S. Air Force Cambridge Research Laboratories, Hanscom Field, Mass., July **1964**, 280 pp.

Hering, W. S., Touart, C. N., and Borden, T. R., Jr., "Ozone Heating and Radiative Equilibrium in the Lower Stratosphere," *Journal of the Atmospheric Sciences*, Vol. 24, No. 4, July **1967**, pp. 402–413.

Howard, John N., Burch, Darrell E., and Williams, Dudley, "Near Infrared Transmission Through Synthetic Atmospheres," *Geophysical Research Paper* No. 40, U.S. Air Force Cambridge Research Center, Hanscom Field, Mass., Nov. **1955**, 244 pp.

Hunt, Barrie G., "Photochemistry of Ozone in a Moist Atmosphere," *Journal of Geophysical Research*, Vol. 71, No. 5, Mar. **1966**, pp. 1385–1398.

Hunt, Barrie G., "Experiments With a Stratospheric General Circulation Model: III. Large-Scale Diffusion of Ozone Including Photochemistry," *Monthly Weather Review*, Vol. 97, No. 4, Apr. **1969**, pp. 287–306.

Hunt, Barrie G., and Manabe, Syukuro, "Experiments With a Stratospheric General Circulation Model: II. Large-Scale Diffusion of Tracers in the Stratosphere," *Monthly Weather Review*, Vol. 96, No. 8, Aug. **1968**, pp. 503–539.

Johnston, H. S., "Reduction of Stratospheric Ozone by Nitrogen Oxide Catalysts From Supersonic Transport Exhaust," *Science*, Vol. 173, No. 3996, Aug. 6, **1971**, pp. 517–522.

Leovy, Conway, "Radiative Equilibrium of the Mesosphere," *Journal of the Atmospheric Sciences*, Vol. 21, No. 3, May **1964**, pp. 238–248.

Leovy, Conway, "Simple Models of Thermally Driven Mesospheric Circulations," *Journal of the Atmospheric Sciences*, Vol. 21, No. 4, July **1964**, pp. 327–341.

Lindzen, Richard S., and Goody, Richard, "Radiative and Photochemical Processes in Mesospheric Dynamics: Part I, Models for Radiative and Photochemical Processes," *Journal of the Atspheric Sciences*, Vol. 22, No. 4, July **1965**, pp. 341–348.

London, Julius, "The Average Distribution and Time Variation of Ozone in the Stratosphere and Mesosphere," Space Research Vol. 7: *Proceedings of the 7th International Space Science Symposium, Vienna, Austria, May 10–18, 1966*, North Holland Publishing Company, Amsterdam, **1967**, pp. 172–185.

Manabe, Syukuro, and Hunt, Barrie G., "Experiments With a Stratospheric General Circulation Model: I. Radiative and Dynamic Aspects," *Monthly Weather Review*, Vol. 96, No. 8, Aug. **1968**, pp. 477–502.

Murgatroyd, R. J., "Winds and Temperatures Between 20 km and 100 km—a Review," *Quarterly Journal of the Royal Meteorological Society*, Vol. 83, No. 358, London, England, Oct. **1957**, pp. 417–458.

Murgatroyd, R. J., Hare, F. K., Boville, B. W., Teweles, S., and Kochanski, A., "The Circulation in the Stratosphere, Mesosphere and Lower Thermosphere," *Technical Note* No. 70, World Meteorological Organization, Geneva, Switzerland, **1965**, 206 pp.

Murgatroyd, R. J., and Singleton, F., "Possible Meridional Circulations in the Stratosphere and Mesosphere," *Quarterly Journal of the Royal Meteorological Society*, Vol. 87, No. 372, London, England, Apr. **1961**, pp. 125–135.

Newell, Reginald E., "Preliminary Study of Quasi-Horizontal Eddy Fluxes From Meteorological Rocket Network Data," *Journal of the Atmospheric Sciences*, Vol. 20, No. 3, May **1963**, pp. 213–225.

Oort, Abraham H., "On the Energy Cycle in the Lower Stratosphere," *Scientific Report* No. 9, Contract No. AT(30–1)2241, Planetary Circulations Project, Department of Meteorology, Massachusetts Institute of Technology, **1963**, 122 pp.

Prabhakara, Cuddapah, "Effects of Non-Photochemical Processes on the Meridional Distribution and Total Amount of Ozone in the Atmosphere," *Monthly Weather Review*, Vol. 91, No. 9, Sept. **1963**, pp. 411–431.

Rao, V. R. Krishna, "A Numerical Experiment on the Steady State Meridional Structure of the Stratosphere," Ph.D thesis, Department of Meteorology, McGill University, **1970**, 229 pp.

Reed, Richard J., and German, Kenneth E., "A Contribution to the Problem of Stratospheric Diffusion by Large-Scale Mixing," *Monthly Weather Review*, Vol. 93, No. 5, May **1965**, pp. 313–321.

Reynolds, O., "On the Dynamical Theory of Incompressible Viscous Fluids and the Determination of the Criterion," *Philosophical Transactions of the Royal Society of London*, Ser. A., Vol. 136, **1894**, pp. 123–164.

Richtmyer, R. D., "Difference Methods for Initial-Value Problems," New York, N. Y., *Interscience Publishers*, **1957**, 238 pp.

Smagorinsky, Joseph, Manabe, Syukuro, and Holloway, J. Leith, Jr., "Numerical Results From a Nine-Level General Circulation Model of the Atmosphere," *Monthly Weather Review*, Vol. 93, No. 12, Dec. **1965**, pp. 727–768.

Teweles, Sidney, "Stratospheric-Mesospheric Circulation," *Research in Geophysics*, Vol. 2, No. 19, Solid Earth and Interface Phenomena, M.I.T. Press, Cambridge, Mass., **1964**, p. 509.

Thompson, Philip D., *Numerical Weather Analysis and Prediction*, The MacMillan Company, New York, N. Y., **1961** 170 pp.

Vincent, D. G., "Mean Meridional Circulations in the Northern Hemisphere Lower Stratosphere During 1964 and 1965," *Quarterly Journal of the Royal Meteorological Society*, Vol. 94, No. 401, London, England, July **1968**, pp. 333–349.

Walshaw, C.D., "Integrated Absorption by the 9.6 Band of Ozone," *Quarterly Journal of the Royal Meteorological Society*, Vol. 83, No. 357, London, England, July **1957**, pp. 315–321.

Williams, G. P., and Davies, D. R., "A Mean Motion Model of the General Circulation," *Quarterly Journal of the Royal Meteorological Society*, Vol. 91, No. 390, London, England, Oct. **1965**, pp. 471–489.

Wulf, Oliver R., and Deming, L. S., "The Theoretical Calculation of the Distribution of the Photochemically-Formed Ozone in the Atmosphere," *Journal of Terrestrial Magnetism and Atmospheric Electricity*, Vol. 41, No. 3, The Johns Hopkins Press, Baltimore, Md., Sept. **1936**, pp. 299–310.

[*Received March 24, 1972; revised March 2, 1973*]